

On The Unusual Variability of 2MASS J06195260–2903592: A Long-Lived Disk around a Young Ultracool Dwarf

MICHAEL C. LIU,^{1,2} EUGENE A. MAGNIER,¹ ZHOUJIAN ZHANG,^{2,3} ERIC GAIDOS,^{4,1} TRENT J. DUPUY,⁵ PENGYU LIU,⁶
BETH A. BILLER,⁶ JOHANNA M. VOS,⁷ KATELYN N. ALLERS,⁸ JASON T. HINKLE,¹ BENJAMIN J. SHAPPEE,¹
SAGE N. L. CONSTANTINOU,¹ MITCHELL T. DENNIS,¹ AND KENJI S. EMERSON¹

¹*Institute for Astronomy, University of Hawai‘i, 2680 Woodlawn Drive, Honolulu HI 96822*

²*Visiting Astronomer at the Infrared Telescope Facility, which is operated by the University of Hawai‘i under contract 80HQTR19D0030 with the National Aeronautics and Space Administration.*

³*The University of Texas at Austin, Department of Astronomy, 2515 Speedway C1400, Austin, TX 78712, USA*

⁴*Department of Earth Sciences, University of Hawai‘i at Manoa, 1680 East-West Rd, Honolulu, HI 96822, USA*

⁵*Institute for Astronomy, University of Edinburgh, Royal Observatory, Blackford Hill, Edinburgh, EH9 3HJ, UK*

⁶*SUPA, Institute for Astronomy, Royal Observatory, University of Edinburgh, Blackford Hill, Edinburgh EH9 3HJ, UK; Centre for Exoplanet Science, University of Edinburgh, Edinburgh EH9 3HJ, UK*

⁷*Department of Astrophysics, American Museum of Natural History, Central Park West at 79th Street, NY 10024, USA*

⁸*Department of Physics and Astronomy, Bucknell University, Lewisburg, PA 17837*

(Accepted for publication in AJ, August 22, 2022)

ABSTRACT

We present the characterization of the low-gravity M6 dwarf 2MASS J06195260–2903592, previously identified as an unusual field object based on its strong IR excess and variable near-IR spectrum. Multiple epochs of low-resolution ($R \approx 150$) near-IR spectra show large-amplitude (≈ 0.1 – 0.5 mag) continuum variations on timescales of days to 12 years, unlike the small-amplitude variability typical for field ultracool dwarfs. The variations between epochs are well-modeled as changes in the relative extinction ($\Delta A_V \approx 2$ mag). Similarly, Pan-STARRS1 optical photometry varies on timescales as long as 11 years (and possibly as short as an hour) and implies similarly amplitude of A_V changes. *NEOWISE* mid-IR light curves also suggest changes on 6-month timescales, with amplitudes consistent with the optical/near-IR extinction variations. However, near-IR spectra, near-IR photometry, and optical photometry obtained in the past year indicate the source can also be stable on hourly and monthly timescales. From comparison to objects of similar spectral type, the total extinction of 2MASS J0619–2903 seems to be $A_V \approx 4$ – 6 mag, with perhaps epochs of lower extinction. *Gaia* EDR3 finds that 2MASS J0619–2903 has a wide-separation ($1'2 = 10450$ AU) stellar companion, with an isochronal age of 31_{-10}^{+22} Myr and a mass of $0.30_{-0.03}^{+0.04} M_\odot$. Adopting this companion’s age and EDR3 distance (145.2 ± 0.6 pc), we estimate a mass of 0.11 – $0.17 M_\odot$ for 2MASS J0619–2903. Altogether, 2MASS J0619–2903 appears to possess an unusually long-lived primordial circumstellar disk, perhaps making it a more obscured analog to the “Peter Pan” disks found around a few M dwarfs in nearby young moving groups.

Keywords: M dwarf stars (982), Circumstellar matter (241)

1. INTRODUCTION

We present here characterization of the M6 dwarf 2MASS J06195260–2903592 (hereinafter 2MASS J0619–2903). This object was found by Cruz et al. (2003) as part of their 2MASS-based search for ultracool members of the solar neighborhood. They noted that the object’s red optical spectrum showed signs of low gravity (i.e., youth), based

on weakness of the CaH (6750–7050 Å) and K I $\lambda\lambda$ 7665, 7669 Å absorption features relative to the M6 optical standard and similarity to the members of the TW Hyd Association (10 ± 3 Myr; Bell et al. 2016) known at the time. (Cruz & Gagné 2014 classify the optical spectrum as M6 β .) Cruz et al. estimated a rough distance of 100 pc, and Gaia EDR3 finds it resides at 148 ± 5 pc (Gaia Collaboration et al. 2016, 2021).^{1,2}

Allers & Liu (2013) classified the near-IR spectrum of 2MASS J0619–2903 as M5. Though this subclass was outside the early-type boundary of their quantitative gravity classification scheme, they noted that the spectrum qualitatively showed low-gravity features in comparison to field M5 dwarfs. Their low-resolution ($R \sim 150$) spectrum, obtained on UT 2008 November 28, showed an unusually red near-IR continuum suggestive of significant circumstellar reddening. Allers & Liu estimated an extinction of $A_V = 6.5$ mag from comparison with young objects of similar spectral type. As the Schlegel et al. (1998) dust map suggests very little extinction along this line of sight ($A_V \lesssim 0.2$ mag), such extinction is expected to be circumstellar, consistent with the object’s very-red near-IR continuum and the finding from Lyons et al. (2012) of the object having a mid-IR excess.

Liu et al. (2016) obtained a second low-resolution near-IR spectrum on UT 2015 December 24, with the goal of higher S/N compared to the 2008 spectrum from Allers & Liu (2013). Liu et al. classified their new spectrum as M6 VL-G. Surprisingly, the two spectra were noticeably different, with the 2015 data being significantly bluer than the 2008 data. Zhang et al. (2018) analyzed the two near-IR spectra using their system for determining both spectral type and reddening. They found spectral types of $M5.3\pm 0.9$ and $M5.8\pm 0.9$ and extinctions of $A_V = 6.3 \pm 4.0$ and 5.5 ± 4.0 mag for the 2008 and 2015 spectra, respectively. (The ± 4 mag uncertainty in A_V adopted by the Zhang et al. methodology is conservative, based on the intrinsic scatter in the colors for ultracool dwarfs. The two spectra clearly have different continua.)

This paper is a follow-up study of 2MASS J0619–2903, which verifies its near-IR spectroscopic variability and demonstrates its photometric variability at optical and mid-IR wavelengths. Section 2 presents new multi-epoch spectra and photometry. Section 3 discusses the properties of the new observations, and Section 4 concludes with a discussion of the system’s properties and comparison with other known objects.

2. OBSERVATIONS

2.1. Spectroscopy: IRTF/SpeX

We obtained more near-IR (0.8–2.5 μm) spectroscopy for 2MASS J0619–2903 using the NASA Infrared Telescope Facility (IRTF) on the summit of Mauna Kea, Hawaii. We obtained data on 5 separate nights spanning about 4 months from November 2020 to early April 2021 and then an additional 2 epochs in Jan/Feb 2022. We used the facility spectrograph SpeX (Rayner et al. 2003) in prism mode with the 0.5'' slit, which provided an average spectral resolution ($R \equiv \Delta\lambda/\lambda$) of ≈ 150 . We dithered in an ABBA pattern on the science target to enable sky subtraction during the reduction process. For each epoch, we obtained calibration frames (arcs and flats) and observed an A0 V star contemporaneously for telluric calibration. All spectra were reduced using the Spextool software package (Vacca et al. 2003; Cushing et al. 2004). We determined near-IR spectral types and Allers & Liu (2013) gravity classifications using the reddening-independent modification to the Allers & Liu system developed by Zhang et al. (2018). The spectral types between the different epochs are consistent with each other given the typing uncertainties. Most of the spectra have VL-G gravity classification, while the two INT-G epochs have spectra with S/N below the $\gtrsim 50$ –75 needed for robust gravity classification, so there is no clear evidence for gravity class variability. Table 1 summarizes our observations and derived measurements. Figure 1 plots our new spectra and the published spectra, totalling 9 epochs spanning about 12.5 years.

2.2. Photometry from Wide-Field Sky Surveys

We examined several multi-epoch wide-field surveys to search for photometric variability of 2MASS J0619–2903. Photometry from the Pan-STARRS1 (PS1) telescope was extracted from observations obtained in two periods. Observations prior to 2014 April 1 were performed as part of the Pan-STARRS1 Science Consortium 3π Survey (Chambers et al. 2016). After 2014 April 1, observations were performed as part of its NASA-funded mission to search for near-Earth asteroids. Exposures from both periods were photometrically calibrated with respect to the

¹ The discrepancy arises because the source is significantly brighter than (old) field objects of similar spectral type, e.g., its K_S -band absolute magnitude of 7.60 ± 0.08 mag is ≈ 1.6 mag brighter than field M6 dwarfs but similar to M6 VL-G objects (Liu et al. 2016).

² Cruz et al. noted that another low-gravity late-M dwarf in their sample, 2MASS J0608528–275358, is close on the sky to 2MASS J0619–2903 but with a discrepant distance estimate of 30 pc. EDR3 places this object at 44.2 ± 0.3 pc, so indeed the two sources are not physically associated.

Pan-STARRS internal photometry database as described by Magnier et al. (2020a). Exposures from these two periods that overlapped the field of interest were ingested into a stand-alone photometry database following the process outlined in Magnier et al. (2020b). All measurements associated with the target were extracted from the database. Of 227 measurements available, 5 were rejected due to $\text{PSF_QF} < 0.85$ and 2 were rejected on the basis of bad photometry flag bits `SIZE_SKIPPED` and `MOMENTS_FAILURE` (Magnier et al. 2020c). For epochs where 2MASS J0619–2903 was not detected by the standard processing, the mask images were examined. The PSF-weighted mask fraction (equivalent to PSF_QF) was measured for the position of the target from each exposure. All values fell into two ranges, < 0.05 and > 0.95 . For the former, the source position was masked, and thus the source could not have been detected. For the latter, then 2MASS J0619–2903 should have been detected if it were bright enough. The 5σ detection limit was calculated as described in Magnier et al. (2020c), with artificial sources injected into the image near the expected detection threshold and recovered if possible by the detection algorithm. Figure 2 shows the PS1 light curves spanning 2010 February 16 to 2021 February 22, giving both detections and 5σ upper limits. Variability is seen on a wide range of timescales, from intra-night to over the entire 11-year dataset.

The ongoing All-Sky Automated Survey for SuperNovae (ASAS-SN; Shappee et al. 2014; Kochanek et al. 2017) and the Asteroid Terrestrial-impact Last Alert System (ATLAS; Tonry et al. 2018) provide wide-field data with less sensitivity than PS1 but much higher cadence. Neither of these surveys is sensitive enough to detect 2MASS J0619–2903’s photosphere, but we examined their datastream to look for bright flaring. ASAS-SN observed 2MASS J0619–2903 for a total of 956 epochs in V band (358 epochs) or g band (598 epochs) from UT 2013 November 1 through UT 2021 December 6. The median V - and g -band 5σ upper limits are 17.9 and 18.4 mag, respectively, without any detections.

ATLAS observed 2MASS J0619–2903 for a total of 98 epochs in the c band (420–650 nm) and 308 epochs in the o band (560–820 nm) between UT 2015 October 22 and UT 2021 December 3 at a typical cadence of 4 days. There are no ATLAS detections, with median 5σ upper limits of 20.2 in the c band and 19.6 mag in the o band.

No photometric variability is reported in *Gaia* DR2 for 2MASS J0619–2903 from the `phot_variable_flag` field. Guidry et al. (2021) have developed a method to detect variable sources from the *Gaia* photometry catalogs based solely on the reported G -band fluxes, flux errors, and number of observing epochs. Computing their `VARINDEX` statistic (see their Appendix E) for DR2 and EDR3 data gives values of 0.075 and 0.048, respectively. For comparison, they find values of >0.007 and >0.0027 for the top 1% of the most variable sources in their white dwarf sample. The values for 2MASS J0619–2903 far exceed these criteria, suggesting 2MASS J0619–2903 is variable in G band.

The AllWISE variability flag is `11nn`, indicating no significant evidence for mid-IR variability over the two epochs of observations in 2010–2011. CatWISE2020 (Marocco et al. 2021) provides 14 epochs of data taken from 2010–2018 and reports p -values for $W1$ and $W2$ of 0.027 and 9.8×10^{-7} , respectively, suggesting significant mid-IR variability, especially in the longer wavelength band. We examine the individual epochs in Section 3.2.2.

2.3. LCOGT Optical Photometric Monitoring

The 2MASS J0619–2903 field was imaged through the Sloan gri and Pan-STARRS z passbands with the Spectral camera on the Faulkes-South 2-m telescope of the Las Cumbres Global Telescope network (LCOGT, Brown et al. 2013) at 30 epochs between UT 2021 December 29 and 2022 February 15. The Spectral camera provides a $10.5' \times 10.5'$ field of view with $0.152''$ pixels binned to 2×2 . Integration times were 200, 35, 40, and 160 sec in the respective $griz$ bandpasses to achieve a photon-noise $S/N=200$ in all but the g band, for which we expect $S/N \approx 20$ for 2MASS J0619–2903. Bias removal, flat-fielding, source identification, and aperture photometry were performed by the automated BANZAI pipeline (McCully et al. 2018). The faintness of 2MASS J0619–2903 in g -band meant that it was usually not detected by BANZAI, and thus aperture photometry was performed directly at the location of the source. Relative time-series photometry was calculated by matrix solution of a set of linear equations describing the relation between instrumental magnitudes and apparent (top of the atmosphere) magnitudes with observation zero-points, a second-order (color-dependent) extinction coefficient, and an instrument-specific color-term. (We used $G_{BP} - G_{RP}$ colors for the latter two terms.) Reference stars are selected based on brightness, color, and lack of significant variability as estimated by *Gaia*, and excluding 2MASS J0619–2903 itself. The residuals of each individual reference star are calculated after solution of the matrix relation; the reference stars with the largest residuals (after subtraction of formal errors) are removed from the fit; and the fit re-calculated. This iteration continues until the median error in the zeropoints, which dominates the errors in the final photometry, is minimized.

Figure 3 shows the relative photometry in each of the four passbands. Variability between the passbands is not consistent, suggesting that the origin is not astrophysical, except perhaps for the case of the Sloan r filter. This

bandpass contains the $H\alpha$ line, which is likely variable given the star’s youth. The overall variability (median absolute deviation) in the *griz* passbands is 0.30, 0.11, 0.045, and 0.10 mag, respectively, but this is not much different than the median formal errors (photon noise and zero-point error added in quadrature) of 0.22, 0.08, 0.038, and 0.036 mag, respectively. The corresponding reduced χ^2 values for each filter’s photometry relative to the mean values are 4.0, 4.0, 1.7, and 14.6, suggesting general constancy in flux except for *z*-band (which could be affected by fringing and thereby leading to a high $\tilde{\chi}^2$ value). We suspect that *g*-, *r*-, and *z*-band uncertainties are actually somewhat underestimated due to data systematics and that the star was not significantly ($\gtrsim 0.1$ mag) variable during the LCOGT observations.

2.4. NTT/SOFI Near-IR Photometric Monitoring

We obtained near-continuous IR photometry of 2MASS J0619–2903 on two consecutive half-nights with the Son of ISAAC (SOFI) instrument, the IR spectrograph and imaging camera on the 3.58-m ESO New Technology Telescope (NTT). We observed 2MASS J0619–2903 in J_S band on the night of 2022 February 19 UT with a total elapsed time of 3.9 hours and interleaved in J_S , H and K_S bands on the following night of 2022 February 20 UT with a total elapsed time of 4.2 hours. The J_S band has a central wavelength of 1.240 μm and a width of 0.290 μm ; the H band is at 1.653 μm with a width of 0.297 μm ; the K_S band is at 2.162 μm with a width of 0.275 μm . The field of view of SOFI is $4.92' \times 4.92'$ with a pixel scale of 0.288"/pixel. We used an ABBA nod pattern during the observations in order to subtract the background, with three 60-second images taken at each nod position. The observations were obtained entirely at airmass less than 2. The seeing was 0.8–1.3" on the first night and 0.6–1.2" on the second night.

We followed the same data reduction as Vos et al. (2019). We corrected the inter-quadrant row crosstalk and applied flat-fielding and illumination corrections. Frames of one nod were subtracted with the frame of the opposite nod closest in time to remove the background. Then we applied aperture photometry to the stars detected in the field. We selected a fixed aperture radius that was similar to the median FWHM of all stars and also that minimized the photometric noise of the target light curve. The photometric noise was measured by the same method used in Radigan et al. (2014), namely the standard deviation of the light curve subtracted by a shifted light curve of itself with one time stamp difference, divided by $\sqrt{2}$. The final aperture radius we used for the 2022-02-19 J_S -band data was 1.0" and was 1.15" for the 2022-02-20 J_S -, H - and K_S -band data. The light curve extracted at each nod position was normalized by its median. We used the iterative algorithm of Radigan et al. (2014) to select a set of reference stars that were not variable after being detrended by other reference stars. Then we took the median light curve of these reference stars as the calibration light curve. The light curve of the target was divided by this calibration light curve in order to remove the systematic variability caused by the instrument and the atmosphere. Figure 4 shows the final detrended light curves. Some low-amplitude ($\approx 1\%$) variability appears to be present over the ≈ 4 hour observations, especially in the J_S -band light curve from the first night and perhaps the K_S -band light curve of the second night, and is plausibly due to photospheric inhomogeneities, e.g., a hot/cool spot, instead of indicating hour-scale extinction variations.

We analyzed the detrended light curve for each filter using the Lomb-Scargle periodogram (LS; Lomb 1976; Scargle 1982) but did not detect a significant periodicity within the observing duration. We also ran the LS periodogram on the joined two-night light curve of J_S band, finding a peak power at 4.11 hours. To check false-positive detections caused by our observation cadence, we also ran the LS periodogram on our observation window function, which is the same time series as the light curve but with a unit value of 1 (VanderPlas 2018). Though the 4.11 hour period did not correspond a strong peak in the window function’s periodogram, the joined J_S -band periodogram also has peaks of similar power at other similar periods, so we do not consider this to be a definitive periodicity detection. A longer-duration continuous dataset would be valuable.

3. ANALYSIS

3.1. Spectroscopy

3.1.1. Variable Near-IR Extinction

Visual examination of the near-IR spectra suggests that the observed changes in the continuum slope could be due to extinction changes. To quantify this, we measured the relative extinction between different epochs, using the highest S/N spectrum (from December 2015) as a template. For each of the other epochs, we fitted the template to the data assuming the template had been reddened by A_V that followed the Fitzpatrick (1999) extinction law with the usual $R = A_V/E(B - V) = 3.1$, along with a wavelength-independent scaling factor to account for differences in the overall flux calibration due to varying slit losses and source brightness compared to the 2015 template. We performed the fit using a grid of A_V and scale factors, adopting the values corresponding to the lowest χ^2 . (We also tried fits with R as

an additional free parameter. The resulting constraints were poor, as expected given the limited wavelength range of our spectra.) The formal uncertainties on A_V from the fits were negligible, but conservatively assuming an uncertainty for SpeX spectra’s continua of $\Delta(J - K) = 0.05$ mag (e.g. Dupuy & Liu 2012; Radigan et al. 2012) would imply an uncertainty of $\sigma(A_V) = 0.3$ mag. For our four epochs from 2021 and 2022, the fits resulted in a negative value for A_V , as expected given that these epochs’ spectra are bluer than the 2015 template. Table 1 includes the fitting results, and Figure 5 shows the dereddened spectra. The latter indicates that the differences between the near-IR spectra are consistent with changes in their relative extinction by $\Delta A_V \approx 2$ mag.

Note that the timescale for extinction changes can be quite heterogenous. For instance, the two observations from 2020 December have very similar inferred extinctions while the two from 2021 April have notably different ones, even though each pair of observations is separate by only a few days. In contrast, our final 3 epochs of spectra, spanning 10.5 months, have nearly consistent spectra, suggesting the system may have been in a steady state for nearly the past year.

3.1.2. Optical Spectrum

Comparison of the Cruz et al. (2003) optical spectrum to the solar-metallicity M6 template from PyHammer v2.0 (Kesseli et al. 2017) supports the notion that 2MASS J0619–2903 has significant reddening. Figure 6 shows that a reddening of $A_V = 4.3$ mag is needed to make the spectra agree, an extinction roughly in accord with the published $A_V \approx 6$ mag estimates.³

Using the Cruz et al. (2003) optical spectrum, we measure an equivalent width (EW) of -7.4 ± 0.4 Å for the H α emission, from simple Gaussian fitting assuming a constant continuum level and Monte Carlo error propagation. For more direct comparison with the literature, we also measure EW(H α) of -8.9 ± 2.7 Å following the definitions of the emission line and its continuum level from Schmidt et al. (2015) (with the lower S/N of this measurement compared to direct Gaussian fitting being due to the narrow continuum bands.) For spectral types M5 and M6, Barrado y Navascués & Martín (2003) set 18.0 and 24.1 Å, respectively, as the H α equivalent width that distinguishes objects with strong chromospheric activity from those with accretion, based on low-resolution optical spectra for members of star-forming regions and young ($\lesssim 125$ Myr) clusters. Thus 2MASS J0619–2903 is not clearly accreting. Also, the measured EW(H α) for 2MASS J0619–2903 is not particularly distinctive for age estimation, as mid-M dwarfs with ages spanning $\sim 10^{7-9}$ yr can show such values (e.g., Figure 5 of Kiman et al. 2021).

3.2. Photometry

3.2.1. Optical Variability

In contrast to our NTT/SOFI data, the PS1 light curves suggest possible short-timescale (≈ 1 -hour) variability. Figure 7 shows the time blocks with 4 or more photometry points separated by < 1 hour, taken in the same filter, and having significant non-constant flux (specifically, having p-values $< 10^{-4}$, indicating the block’s data are not consistent with a constant flux given the measurement uncertainties). Such rapid changes could be due to intrinsic photospheric variability (cool/hot spots or localized accretion features; e.g., Herbst et al. 1994; Becker et al. 2011) or extrinsic variability due to small-scale inhomogeneities in the circumstellar material. We caution that some deviations may be due to instrumental systematics, e.g., when the object falls on two different detectors on the same night, as the PS1 3π Survey observing strategy was not optimized for high-precision short-term photometric monitoring. High-cadence, multi-wavelength monitoring would help constrain the possible scenarios.

Figure 2 shows the PS1 z_{P1} - and y_{P1} -band photometry changes are seemingly correlated over the many years of data, namely both become faint or bright at the same time. The non-simultaneity of the observations precludes a more definitive statement, as photometry in the two filters were typically taken 1–2 weeks apart during the 3π Survey.⁴ Over all 11 years of data, the full ranges of the z_{P1} and y_{P1} magnitudes are 0.6 and 0.7 mag, respectively, corresponding to A_V changes of 1.1 and 1.8 mag using the Tonry et al. (2012) extinction curve.⁵ Similarly, the full ranges of r_{P1} and

³

In principle, we should also compare to unreddened young M6 objects to gauge the extinction, but there is a paucity of suitable data. The RIZzo spectral library (Cruz & Gagné 2014) only contains two young objects with M6 spectral types besides 2MASS J0619–2903. 2MASS 0557–1359 (optical spectral type M6: γ in RIZzo; M7 in Cruz et al. 2007) is a somewhat enigmatic young field object with a near-IR spectrum that shows lower surface gravity (i.e., younger age) than most field objects and a very bright absolute magnitude (Liu et al. 2016), making it a poor comparison object. 2MASS 2234+4041 (optical spectral type M6: δ) is a very young (~ 1 Myr) member of the LkH α 233 star-forming group (Allers et al. 2009), so its optical spectrum is likely to differ from a young field M6 dwarf due to both extinction and gravity effects. Best et al. (2018) show that the optical PS1 colors for young late-M dwarfs are similar to those of field late-M dwarfs, so using the PyHammer v2.0 template is a reasonable choice for estimating the extinction of 2MASS J0619–2903.

⁴

There are only 2 blocks of PS1 photometry for which multi-filter data were obtained ≤ 2 days apart, both involving the z_{P1} and y_{P1} filters. The two epochs give colors of $z_{P1}-y_{P1}$ of 0.51 ± 0.02 mag ($\langle \text{MJD} \rangle = 55634.8$, $\Delta t = 1.1$ days) and 0.62 ± 0.02 mag ($\langle \text{MJD} \rangle = 56297.4$, $\Delta t = 2.0$ days).

⁵

The Tonry et al. extinction curve for PS1 depends on the $g_{P1}-i_{P1}$ color, though the dependence is very weak for the standard bandpasses. Using the typical $g_{P1} - i_{P1}$ color for M5–M6.9 dwarfs from Best et al. (2018), the extinction values (A_λ) in $g_{P1} r_{P1} i_{P1} z_{P1} y_{P1}$ are factors of 1.10, 0.80, 0.60, 0.48, and 0.40 different from that of V band (A_V).

i_{P1} magnitudes are 1.0 and 0.7 mag, respectively, corresponding to A_V changes of 0.8 and 0.4 mag (though r_{P1} could be affected by variable $H\alpha$ emission). Such extinction variations are comparable in amplitude to those inferred from the near-IR spectra (Table 1).

In addition to variability, the PS1 light curves suggest there might be periods of very low/no extinction. The mean z_{P1} and y_{P1} magnitudes from the 3π Survey were 17.524 ± 0.006 and 16.933 ± 0.017 mag, respectively, giving a color of $z_{P1} - y_{P1} = 0.59 \pm 0.02$ mag, similar to the median color of 0.44–0.51 mag for M5.0–M6.9 dwarfs from Best et al. (2018). For the same spectral type range, Best et al. tabulate median colors of $r_{P1} - i_{P1} = 1.9 - 2.1$ mag and $i_{P1} - z_{P1} = 0.9 - 1.0$ mag, comparable to the colors of $r_{P1} - i_{P1} = 1.71 \pm 0.05$ mag and $i_{P1} - z_{P1} = 0.967 \pm 0.008$ mag computed from the non-simultaneous 3π Survey photometry, i.e., no strong reddening. (Note there are relatively few epochs of i_{P1} data from the 3π Survey, as many of the pointings resulted in the source landing on a masked portion of the detector.) To further illustrate this, Figure 2 shows the predicted magnitudes of 2MASS J0619–2903 assuming the brightest y_{P1} -band detection represents the unextincted photosphere and using the Best et al. (2018) colors for M6 dwarfs. The brightest detections in the other bands are just consistent with the predicted unextincted magnitudes, suggesting some epochs have low extinction.

The interpretation of the bluest (g_{P1} -band) detections is unclear. There are two modest ($S/N = 6$ and 8) detections of 2MASS J0619–2903, both of which are verified by visual inspection of the reduced images. Both of these images were obtained as one of a pair of images taken 17 minutes apart, given the standard PS1 3π Survey observing strategy of searching for fast-moving asteroids by taking pairs of closely-spaced exposures. For the detection on MJD 55895.49280 of 21.77 ± 0.16 mag, the immediately preceding image had a 5σ detection limit of $g_{P1}=21.70$ mag, and visual inspection of the smoothed image shows no sign of any counterpart. For the detection on MJD 56662.38760 of 21.36 ± 0.12 mag, 2MASS J0619–2903 was not detected to a depth of $g_{P1}=21.5$ mag in the other image of the pair, which we corroborate with visual inspection. This suggests that g -band variability of $\gtrsim 0.2$ mag occurred on ≈ 20 minute timescales, consistent with flaring activity of field M dwarfs (e.g. Davenport et al. 2014; Davenport 2016).

However, given the large inferred extinction for the source, the photosphere should not have been detected at all in g_{P1} band. The Best et al. (2018) compilation of M dwarfs shows that M6 dwarfs have $g_{P1} - K_S$ colors of 7.2 ± 0.3 mag. Assuming $A_V = 6$ mag ($A_{g_{P1}} \approx 7$, $A_K = 0.7$ mag), the 2MASS K_S -band photometry of 2MASS J0619–2903 would imply $g_{P1} \approx 20 \pm 0.3$ mag and ≈ 27 mag for its unextincted and extincted photosphere, respectively. Thus if the large optical extinctions inferred by Allers & Liu (2013) and Zhang et al. (2018) from the near-IR spectra are typical, then 2MASS J0619–2903 is expected to be undetected by PS1 in g_{P1} band, given the 5σ limiting magnitudes of 22.0 and 23.3 mag for the PS1 single-epoch and stacked exposures, respectively. Thus the two g_{P1} -band detections can be attributed to flaring activity. The implied flare amplitudes would be $\Delta g_{P1} \gtrsim 4$ mag, consistent with the largest flares seen for field M dwarfs (Schmidt et al. 2019). On the other hand, the unextincted photosphere is well above the g_{P1} -band limiting magnitudes, and thus the two $g_{P1} \approx 21.5$ mag detections could arise from epochs when the photosphere was only lightly extincted. More intensive multi-band monitoring could distinguish between flaring and extinction variations.

3.2.2. Mid-IR Variability

We investigated the mid-IR variability of 2MASS J0619–2903 indicated by CatWISE2020 (Section 2.2) by examining the individual single-exposure photometry reported by the NEOWISE Reactivation Mission (Mainzer et al. 2014; NEOWISE Team 2020), spanning 2014 March 24 to 2020 September 30. The object is well detected in individual exposures, with S/N of 34 and 20 in $W1$ and $W2$, respectively. Following the recommendations in Cutri et al. (2015), we removed any data with non-zero confusion flags (`cc_flags`), low quality scores (`qual_frame=0` or `qi_fact=0`), small distance from the South Atlantic Anomaly (`saa_sep<5`), or close to the moon (`moon_masked≠0`). We also removed epochs with poor reduced χ^2 values for the profile-fit photometry ($\bar{\chi}^2 > 6$), though these were relatively few after applying the aforementioned criteria. Figure 8 plots the NEOWISE light curves.

These data probe two distinct timescales, each day-long visit having ≈ 10 –20 exposures and then the visits being spaced 6 months apart. There is not much evidence for significant intra-visit (day-long) variability. Compared to a model of constant flux at each visit, 3 visits of $W1$ data and 2 visits of $W2$ data out of the 14 total visits have p-values $< 1 \times 10^{-3}$. In contrast, there is potential evidence for variability between the 6-month visits, with p-values of $< 1 \times 10^{-6}$ for both $W1$ and $W2$ when comparing the individual visits’ weighted averages to a model of constant flux during all 14 visits.

To investigate further, we retrieved the *NEOWISE* single exposures for all sources within 1° of 2MASS J0619–2903 and having similar (± 0.25 mag) photometry in either *W1* or *W2*. For each bandpass, after applying the same data-quality cuts, we computed the same $\tilde{\chi}^2$ statistics for the intra-visit and inter-visit fluxes as we did for 2MASS J0619–2903. Figure 9 shows the resulting distributions. For intra-visit data, 2MASS J0619–2903 seems unremarkable relative to the comparison sample. In contrast, its inter-visit photometry suggests that it is variable on ~ 6 -month timescales, as its *W1* and *W2* $\tilde{\chi}^2$ values are the 3rd and 4th highest out of all the sources in the field.

Taking the mid-IR variability at face value, the ≈ 0.1 mag changes would correspond to extinction variations of $A_V \approx 2.5 - 4.0$, comparable to the values inferred from our optical/NIR data. Alternatively, the mid-IR variations could also arise from changes in the disk emission, likely from the inner wall location at the dust sublimation radius (e.g. Flaherty et al. 2013). Simultaneous optical/NIR photometry during *NEOWISE*'s future visit of 2MASS J0619–2903 would be valuable to distinguish between variations in extinction and emission.

3.3. Astrometry, Age, and Mass

Gagné et al. (2014) found that the proper motion of 2MASS J0619–2903 suggested possible membership in the Columba moving group. But a preliminary (S/N ≈ 2) parallax from Liu et al. (2016) was inconsistent with the inferred distance of 55 pc if such membership were correct. The BANYAN Σ (Gagné et al. 2018) algorithm finds that this object's Gaia EDR3 astrometry indicates that it is a field object, not belonging to a known young stellar group or association.

We queried *Gaia* EDR3 (Gaia Collaboration et al. 2016, 2021) to search for possible wide companions to 2MASS J0619–2903. Only two stars within 2° (5.1 pc) of 2MASS J0619–2903 have a similar parallax (± 1 mas) and proper motion (± 1 mas yr $^{-1}$). The closer of the two (Gaia EDR3 2898355055033597184, PSO J094.9535–29.0808) is only $1/2$ away and has a parallax within 0.14 mas (0.6σ) and proper motion differing by 0.36 mas yr $^{-1}$ (1.6σ). This star was identified by Kerr et al. (2021) as being young (31_{-10}^{+22} Myr), but not a member of any known or newly identified young associations. This star and 2MASS J0619–2903 have also been noted as a highly likely physical pair by El-Badry et al. (2021) with a chance-alignment parameter < 0.01 . Such pairs have an average chance alignment probability of 0.08%, and the youth of both objects makes them even more unlikely to be a chance alignment. We thus consider 2MASS J0619–2903 to be a physical companion to this star and adopt the star's $\approx 8\times$ more precise parallax and proper motion for the whole system. This places 2MASS J0619–2903 at a distance of 145.2 ± 0.6 pc with a projected separation of 10450 ± 50 AU from its host star. We use the PARSEC v1.2S isochrones (Chen et al. 2015) and the Kerr et al. (2021) age, assuming negligible extinction based on the 3D map of Capitanio et al. (2017), to estimate a mass of $0.30_{-0.03}^{+0.04} M_\odot$ for the primary star using its absolute magnitude of $M_G = 9.970 \pm 0.009$ mag.

The other star found in our 2° -radius query (Gaia EDR3 2898345984062275072) is $1:521$ away and differs significantly in proper motion (0.89 ± 0.03 mas yr $^{-1}$) from 2MASS J0619–2903. At such a large separation (3.8 pc), projection effects of space motion into astrometric measurements are substantial, and indeed we can find a good match with the *UVW* space motion of both this wide object and the 2MASS J0619–2903 system if we assume a radial velocity of 25–30 km/s for all three stars. However, this star is not identified as young by Kerr et al. (2021), even though it would be a $0.44 \pm 0.04 M_\odot$ pre-main sequence star if it were the same age as the 2MASS J0619–2903 system. We thus consider this wider star to be a chance alignment.

The comoving companion of 2MASS J0619–2903 provides an age for the system, enabling a mass estimate using evolutionary models. We use the 2MASS *K_S*-band magnitude and a bolometric correction for young objects from Filippazzo et al. (2015) to estimate the bolometric luminosity of 2MASS J0619–2903. Adopting a uniform age distribution spanning 21–37 Myr, the Baraffe et al. (2015) models give a mass of $0.11 \pm 0.02 M_\odot$ for 2MASS J0619–2903, assuming no extinction and using a Monte Carlo approach to account for the uncertainties in the magnitude, bolometric correction, distance, and age. If we assume an extinction of $A_V = 6$ mag, the resulting mass is $0.17 \pm 0.03 M_\odot$.

4. DISCUSSION

The variability exhibited by 2MASS J0619–2903 is not typical for field late-M dwarfs. Such stars display photometric modulations due to rotation of their spotted photospheres, showing semi-amplitudes of ≈ 0.2 –2.0% and periods of ≈ 1 –100 days, with kinematically older stars tending to have longer periods than kinematically younger stars (Newton et al. 2016, 2018). This differs from the much larger-amplitude (≈ 0.5 mag) optical variability and the near-IR extinction variations shown by 2MASS J0619–2903, with the variability demonstrating timescales spanning days/weeks (IRTF/SpeX and PS1), months (PS1 and *NEOWISE*), and years (PS1). (Our one continuous ≈ 4 -hour dataset from SOFI does show low-amplitude variability consistent with a spot-modulated rotation light curve.)

Around young (~ 30 – 100 Myr) field stars comparable in age to 2MASS J0619–2903, a small fraction ($\sim 1\%$) of stars with debris disks show extremely large IR excesses suggestive of transient collisional events (Balog et al. 2009; Melis et al. 2012; Moór et al. 2021). Some of these show large-amplitude (≈ 30 – 100%) mid-IR variability with systematic trends on \sim year timescales but without any changes in their optical photometry (Meng et al. 2015; Rieke et al. 2021). This is unlike 2MASS J0619–2903, where both optical and mid-IR variability occurs, the variability has a larger amplitude in the optical than the mid-IR, and the mid-IR variability has a ~ 0.1 mag amplitude without any trend – all these suggest that it does not possess a transient debris disk.

Stars in young (≈ 1 – 15 Myr) star-forming regions show a much richer set of variability phenomena, caused by both photospheric and circumstellar sources, which more resemble the behavior of 2MASS J0619–2903. In addition to rotation-induced modulations from cool and hot spots, photometry of young stars exhibits accretion-related fluctuations, variable obscuration/color changes, and quasi-periodic/aperiodic dimming (“dipping”) events with timescales of less than a few days, indicating origins at the photosphere or inner disk (e.g., Herbst et al. 1994; Carpenter et al. 2001; Stauffer et al. 2014; Ansdell et al. 2016). On timescales of \sim years, optical photometry for most young stars is relatively stable, with only a small fraction exhibiting long-term changes due to variable extinction (Grankin et al. 2007, 2008; Rigon et al. 2017; Hambálek et al. 2019). In contrast, long-timescale variability at mid-IR wavelengths is more common (~ 30 – 50% ; e.g., Flaherty et al. 2012; Rebull et al. 2014; Park et al. 2021) and may arise from structure fluctuations in the inner disk, variable accretion, and/or variable extinction. Finally, a few young systems have very complex light curves suggestive of significant occultation by a structured circumstellar or circumplanetary disk, e.g., AA Tau (Bouvier et al. 2013), V409 Tau (Rodriguez et al. 2015), KH 15D (Hamilton et al. 2001; Winn et al. 2006), 1SWASP J140747.93-394542.6 (Mamajek et al. 2012; van Werkhoven et al. 2014) and PDS 110 (Osborn et al. 2017). Continuous monitoring of 2MASS J0619–2903 is needed to determine whether its extinction variations could arise from such exotic configurations, which cannot be discerned from our existing sparse-cadence data.

The overall properties of 2MASS J0619–2903’s circumstellar material suggests a disk in between the primordial disks abundant in young ($\lesssim 10$ Myr) star-forming regions and the debris disks seen around older stars. The inferred A_V values are too large to be associated with a debris disk, where even edge-on systems present little obscuration of the central star, while the H α emission is not strong enough to clearly show ongoing accretion. The AllWISE colors of 2MASS J0619–2903 ($W1 - W2 = 0.43 \pm 0.03$, $W1 - W3 = 1.75 \pm 0.12$ and $W1 - W4 = 4.04 \pm 0.4$ mag) suggest emission from an evolved or full circumstellar disk, instead of a debris disk (Figure 10). (From the nomenclature of, e.g., Espaillat et al. (2012), evolved disks are gas-rich primordial disks in the process of becoming optically thin but which do not possess large gaps or holes like transitional disks.) Note that the wavelength gap between $W2$ - and $W3$ -band photometry means an inner disk gap might not be noticed with the existing photometry.

Substantial disks older than ~ 20 Myr are rare (e.g., Kraus et al. 2014 find a frequency of $< 0.8\%$ for optically thick and thin disks around M dwarfs in the ~ 40 Myr old Tuc-Hor Association), but they do exist. In addition to 2MASS J0619–2903, Allers & Liu (2013) and Liu et al. (2016) identified 3 M dwarfs that straddle the stellar/substellar mass boundary and have strong IR excesses, though these may be very young (\sim Myr) sources based on their absolute magnitudes. V4046 Sgr is a classical T Tauri K5+K7 binary with a gas-rich evolved circumbinary disk (Jensen & Mathieu 1997; Kastner et al. 2008; Rodriguez et al. 2010), belonging to the β Pictoris moving group (~ 25 Myr). Reiners (2009) identified a young, accreting brown dwarf that they suggested to be in the ~ 40 Myr Tuc-Hor Association (and reaffirmed by Gagné et al. 2014); we re-confirmed this object’s Tuc-Hor membership (99.6% probability) using *Gaia* EDR3 astrometry and the radial velocity from Shkolnik et al. (2017) as inputs to the BANYAN Σ algorithm (Gagné et al. 2018). Rodriguez et al. (2013) found two young ($\sim 10 - 100$ Myr) field M dwarfs with strong mid-IR excesses ($W1 - W4 \approx 4$ mag, comparable to 2MASS J0619–2903).⁶ Boucher et al. (2016) identified two young brown dwarfs in the Columba and Tuc-Hor moving groups (~ 40 Myr) with strong accretion and large fractional disk luminosities, and also highlight the Argus (~ 40 Myr) membership of the T Tauri K5+K7 binary FK Ser (Jensen et al. 1996). Silverberg et al. (2016) identified an M dwarf member of the Carina (~ 45 Myr) moving group with a strong *WISE* excess.⁷ Lee et al. (2020) identified an M dwarf member of the Argus (~ 55 Myr) moving group with a strong

6

Rodriguez et al. (2013) find possible Columba (~ 40 Myr) membership for these two sources, 2MASS J02590146–4232204 and 2MASS J03244056–3904227, based on their kinematics and estimated distances. Using the latest astrometry from *Gaia* EDR3 as input to BANYAN Σ , we find the former is a field object (96.4% probability) and the latter is a Tuc-Hor member (99.7%; also identified as a member by Kraus et al. 2014).

7

Murphy et al. (2018) find this object, WISE J080822.18-644357.3, shows significant mid-IR variability and possesses strong broad H α emission indicating ongoing accretion. Its *WISE* colors suggest a (gas-rich) primordial disk as opposed to a (gas-poor) debris disk, but ALMA observations by Flaherty et al. (2019) establish the disk is gas-poor and has a relatively low disk mass compared to primordial disks. They suggest its circumstellar dust is generated from a collisional cascade of km-sized bodies in the outer (< 16 AU) disk and then migrates inward due to Poynting-Robertson drag to produce the strong mid-infrared excess.

WISE excess and ongoing accretion. Gaidos et al. (2022) identified another M dwarf member of the Carina moving group with a long-lived primordial disk showing ongoing accretion and with a *TESS* light curve having many dipping events. They also suggest such long-lived M dwarf disks could be the progenitors of multi-planet systems around low-mass stars akin to TRAPPIST-1 (Gillon et al. 2017).

Silverberg et al. (2020) brand these long-lived systems as “Peter Pan” disks, namely unusually long-lived ($\gtrsim 20$ Myr) accretion disks around M dwarfs with strong infrared excesses ($K - W4 > 2$ mag). Coleman & Haworth (2020) suggest that for primordial disks around low-mass stars to be so long-lived, the disks must have possessed a combination of rare intrinsic and/or extrinsic properties, such as low disk viscosity, extremely low external photoevaporation (indicating formation in rare environment), and relatively high disk masses. Wilhelm & Portegies Zwart (2022) find that primordial disk lifetimes as long as ~ 50 Myr can only occur around $\lesssim 0.6 M_{\odot}$ stars. 2MASS J0619–2903 fulfills most of the Silverberg et al. criteria for these objects. Though it lacks a clear signature of accretion based on its $\text{EW}(\text{H}\alpha)$, some of the Peter Pan objects would also not be classified as accretors if solely based on their $\text{EW}(\text{H}\alpha)$, as their accretion is only detected with higher resolution spectra that resolves the $\text{H}\alpha$ linewidths. The long-term variability of the Peter Pan sample is not yet known, and 2MASS J0619–2903’s behavior suggests such data could be quite interesting. Overall, 2MASS J0619–2903 may be a more distant, more extincted version of a Peter Pan disk.

More intensive monitoring of 2MASS J0619–2903 is needed to better understand the geometrical, physical, and dynamical nature of its variability. Perhaps most notably, our existing data compilation lacks any long-term continuous monitoring (aside from the 1.5 months of LCOGT optical monitoring, which shows little variability), and a more extensive dataset could explore possible hour-scale variations suggested by the PS1 and NTT photometry. Such a continuous dataset would also help to constrain the orbital radius and spatial structure of the circumstellar material, through periodicity, color, and extinction measurements. Higher spectral resolution optical $\text{H}\alpha$ data would be a sensitive probe for ongoing accretion. Finally, longer wavelength sub-mm/radio observations would better assess the evolutionary state of 2MASS J0619–2903’s disk by measuring the gas and dust masses.

Conducted amidst the turbulence of Fall 2020, the discussions in the ASTR 633 Astrophysical Techniques class at the University of Hawaii were the genesis of this study, resulting in a third epoch of spectra that demonstrated the variability of 2MASS J0619–2903 seen by between the 2008 and 2015 spectra of Liu et al. (2016) continues to persist. We thank John Rayner, Bobby Bus, and Michael Connolly for supporting the IfA graduate students’ IRTF proposal writing and observing time. This work has benefited from discussions with Rob Siverd and John Tonry. This work has benefited from The UltracoolSheet at <http://bit.ly/UltracoolSheet>, maintained by Will Best, Trent Dupuy, Michael Liu, Rob Siverd, and Zhoujian Zhang, and developed from compilations by Dupuy & Liu (2012), Dupuy & Kraus (2013), Liu et al. (2016), Best et al. (2018), and Best et al. (2020). This research has benefitted from the Ultracool RIZo Spectral Library, maintained by Jonathan Gagné and Kelle Cruz. This research was funded in part by the Gordon and Betty Moore Foundation through grant GBMF8550 and by the NSF through grant AST-1518339, both awarded to M. Liu. B. Shappee is supported by NSF grants AST-1908952, AST-1920392 and AST-1911074. E. Gaidos acknowledges support by NASA grants 80NSSC19K0587 (Astrophysics Data Analysis Program) and 80NSSC19K1705 (TESS Guest Observer Cycle 2).

This work has made use of data from the European Space Agency (ESA) mission *Gaia* (<https://www.cosmos.esa.int/gaia>), processed by the *Gaia* Data Processing and Analysis Consortium (DPAC, <https://www.cosmos.esa.int/web/gaia/dpac/consortium>). Funding for the DPAC has been provided by national institutions, in particular the institutions participating in the *Gaia* Multilateral Agreement. This publication makes use of data products from the Wide-field Infrared Survey Explorer (Wright et al. 2010), which is a joint project of the University of California, Los Angeles, and the Jet Propulsion Laboratory/California Institute of Technology, and NEOWISE (Mainzer et al. 2011), which is a project of the Jet Propulsion Laboratory/California Institute of Technology. WISE and NEOWISE are funded by the National Aeronautics and Space Administration. The Pan-STARRS 1 Surveys (PS1) and the PS1 public science archive have been made possible through contributions by the Institute for Astronomy, the University of Hawaii, the Pan-STARRS Project Office, the Max-Planck Society and its participating institutes, the Max Planck Institute for Astronomy, Heidelberg and the Max Planck Institute for Extraterrestrial Physics, Garching, The Johns Hopkins University, Durham University, the University of Edinburgh, the Queen’s University Belfast, the Harvard-Smithsonian Center for Astrophysics, the Las Cumbres Observatory Global Telescope Network Incorporated, the National Central University of Taiwan, the Space Telescope Science Institute, the National Aeronautics and Space Administration under Grant No. NNX08AR22G issued through the Planetary Science Division of the NASA Science Mission Directorate, the National Science Foundation Grant No. AST-1238877, the University of Maryland, Eotvos Lorand University (ELTE), the Los Alamos National Laboratory, and the Gordon and Betty Moore Foundation. Pizza. This work has made use of data from the Asteroid Terrestrial-impact Last Alert System (ATLAS) project. The Asteroid Terrestrial-impact Last Alert System (ATLAS) project is primarily funded to search for near-Earth asteroids through NASA grants NN12AR55G, 80NSSC18K0284, and 80NSSC18K1575; byproducts of the NEO search include images and catalogs from the survey area. This work was partially funded by Kepler/K2 grant J1944/80NSSC19K0112 and HST GO-15889, and STFC grants ST/T000198/1 and ST/S006109/1. The ATLAS science products have been made possible through the contributions of the University of Hawaii Institute for Astronomy, the Queen’s University Belfast, the Space Telescope Science Institute, the South African Astronomical Observatory, and The Millennium Institute of Astrophysics (MAS), Chile. We thank Las Cumbres Observatory and its staff for their continued support of ASAS-SN. ASAS-SN is funded in part by the Gordon and Betty Moore Foundation through grants GBMF5490 and GBMF10501 to the Ohio State University, and also funded in part by the Alfred P. Sloan Foundation grant G-2021-14192. Development of ASAS-SN has been supported by NSF grant AST-0908816, the Mt. Cuba Astronomical Foundation, the Center for Cosmology and AstroParticle Physics at the Ohio State University, the Chinese Academy of Sciences South America Center for Astronomy (CAS- SACA), the Villum Foundation, and George Skestos. This work makes use of observations from the Las Cumbres Observatory global telescope network with Key Project 2020-007 “Catch A Fading Star.” Burrito. Our research has employed the 2MASS data products; NASA’s Astrophysical Data System; and the SIMBAD database operated at CDS, Strasbourg, France. This research has made use of the NASA/IPAC Infrared Science Archive, which is funded by the National Aeronautics and Space Administration and operated by the California Institute of Technology.

Finally, the authors wish to recognize and acknowledge the very significant cultural role and reverence that the summit of Mauna Kea has always had within the indigenous Hawaiian community. We are most fortunate to have the opportunity to conduct observations from this mountain.

Facilities: IRTF (SpeX), ASAS-SN, Pan-STARRS 1, ATLAS, Gaia, WISE, NEOWISE, IRSA, LCOGT (Spectral), NTT (SOFI)

REFERENCES

- Allers, K. N., & Liu, M. C. 2013, *ApJ*, 772, 79, doi: [10.1088/0004-637X/772/2/79](https://doi.org/10.1088/0004-637X/772/2/79)
- Allers, K. N., Liu, M. C., Shkolnik, E., et al. 2009, *ApJ*, 697, 824, doi: [10.1088/0004-637X/697/1/824](https://doi.org/10.1088/0004-637X/697/1/824)
- Ansdell, M., Gaidos, E., Rappaport, S. A., et al. 2016, *ApJ*, 816, 69, doi: [10.3847/0004-637X/816/2/69](https://doi.org/10.3847/0004-637X/816/2/69)
- Balog, Z., Kiss, L. L., Vinkó, J., et al. 2009, *ApJ*, 698, 1989, doi: [10.1088/0004-637X/698/2/1989](https://doi.org/10.1088/0004-637X/698/2/1989)
- Baraffe, I., Homeier, D., Allard, F., & Chabrier, G. 2015, *A&A*, 577, A42, doi: [10.1051/0004-6361/201425481](https://doi.org/10.1051/0004-6361/201425481)
- Barrado y Navascués, D., & Martín, E. L. 2003, *AJ*, 126, 2997, doi: [10.1086/379673](https://doi.org/10.1086/379673)
- Becker, A. C., Bochanski, J. J., Hawley, S. L., et al. 2011, *ApJ*, 731, 17, doi: [10.1088/0004-637X/731/1/17](https://doi.org/10.1088/0004-637X/731/1/17)
- Bell, C. P. M., Mamajek, E. E., & Naylor, T. 2016, 314, 41, doi: [10.1017/S1743921315006213](https://doi.org/10.1017/S1743921315006213)
- Best, W. M. J., Liu, M. C., Magnier, E. A., & Dupuy, T. J. 2020, *aj*, 159, 257, doi: [10.3847/1538-3881/ab84f4](https://doi.org/10.3847/1538-3881/ab84f4)
- Best, W. M. J., Magnier, E. A., Liu, M. C., et al. 2018, *ApJS*, 234, 1, doi: [10.3847/1538-4365/aa9982](https://doi.org/10.3847/1538-4365/aa9982)
- Boucher, A., Lafrenière, D., Gagné, J., et al. 2016, *ApJ*, 832, 50, doi: [10.3847/0004-637X/832/1/50](https://doi.org/10.3847/0004-637X/832/1/50)
- Bouvier, J., Grankin, K., Ellerbroek, L. E., Bouy, H., & Barrado, D. 2013, *A&A*, 557, A77, doi: [10.1051/0004-6361/201321389](https://doi.org/10.1051/0004-6361/201321389)
- Brown, T. M., Baliber, N., Bianco, F. B., et al. 2013, *PASP*, 125, 1031, doi: [10.1086/673168](https://doi.org/10.1086/673168)
- Capitaniao, L., Lallement, R., Vergely, J. L., Elyajouri, M., & Monreal-Ibero, A. 2017, *aap*, 606, A65, doi: [10.1051/0004-6361/201730831](https://doi.org/10.1051/0004-6361/201730831)
- Carpenter, J. M., Hillenbrand, L. A., & Skrutskie, M. F. 2001, *AJ*, 121, 3160, doi: [10.1086/321086](https://doi.org/10.1086/321086)
- Chambers, K. C., Magnier, E. A., Metcalfe, N., et al. 2016, arXiv e-prints, arXiv:1612.05560. <https://arxiv.org/abs/1612.05560>
- Chen, Y., Bressan, A., Girardi, L., et al. 2015, *mnras*, 452, 1068, doi: [10.1093/mnras/stv1281](https://doi.org/10.1093/mnras/stv1281)
- Coleman, G. A. L., & Haworth, T. J. 2020, *MNRAS*, 496, L111, doi: [10.1093/mnrasl/slaa098](https://doi.org/10.1093/mnrasl/slaa098)
- Cruz, K., & Gagné, J. 2014, The Ultracool Rizzo Spectral Library, Zenodo, doi: [10.5281/ZENODO.11313](https://doi.org/10.5281/ZENODO.11313). <https://zenodo.org/record/11313>
- Cruz, K. L., Reid, I. N., Liebert, J., Kirkpatrick, J. D., & Lowrance, P. J. 2003, *AJ*, 126, 2421
- Cruz, K. L., et al. 2007, *AJ*, 133, 439, doi: [10.1086/510132](https://doi.org/10.1086/510132)
- Cushing, M. C., Vacca, W. D., & Rayner, J. T. 2004, *PASP*, 116, 362, doi: [10.1086/382907](https://doi.org/10.1086/382907)
- Cutri, R. M., Mainzer, A., Conrow, T., et al. 2015, Explanatory Supplement to the NEOWISE Data Release Products, Explanatory Supplement to the NEOWISE Data Release Products
- Davenport, J. R. A. 2016, *ApJ*, 829, 23, doi: [10.3847/0004-637X/829/1/23](https://doi.org/10.3847/0004-637X/829/1/23)
- Davenport, J. R. A., Hawley, S. L., Hebb, L., et al. 2014, *ApJ*, 797, 122, doi: [10.1088/0004-637X/797/2/122](https://doi.org/10.1088/0004-637X/797/2/122)
- Dupuy, T. J., & Kraus, A. L. 2013, *Science*, 341, 1492, doi: [10.1126/science.1241917](https://doi.org/10.1126/science.1241917)
- Dupuy, T. J., & Liu, M. C. 2012, *ApJS*, 201, 19, doi: [10.1088/0067-0049/201/2/19](https://doi.org/10.1088/0067-0049/201/2/19)
- El-Badry, K., Rix, H.-W., & Heintz, T. M. 2021, *MNRAS*, 506, 2269, doi: [10.1093/mnras/stab323](https://doi.org/10.1093/mnras/stab323)
- Espaillet, C., Ingleby, L., Hernández, J., et al. 2012, *ApJ*, 747, 103, doi: [10.1088/0004-637X/747/2/103](https://doi.org/10.1088/0004-637X/747/2/103)
- Filippazzo, J. C., Rice, E. L., Faherty, J., et al. 2015, *ApJ*, 810, 158, doi: [10.1088/0004-637X/810/2/158](https://doi.org/10.1088/0004-637X/810/2/158)
- Fitzpatrick, E. L. 1999, *PASP*, 111, 63, doi: [10.1086/316293](https://doi.org/10.1086/316293)
- Flaherty, K., Hughes, A. M., Mamajek, E. E., & Murphy, S. J. 2019, *ApJ*, 872, 92, doi: [10.3847/1538-4357/aaf794](https://doi.org/10.3847/1538-4357/aaf794)
- Flaherty, K. M., Muzerolle, J., Rieke, G., et al. 2013, *AJ*, 145, 66, doi: [10.1088/0004-6256/145/3/66](https://doi.org/10.1088/0004-6256/145/3/66)
- . 2012, *ApJ*, 748, 71, doi: [10.1088/0004-637X/748/1/71](https://doi.org/10.1088/0004-637X/748/1/71)
- Gagné, J., Lafrenière, D., Doyon, R., Malo, L., & Artigau, É. 2014, *ApJ*, 783, 121, doi: [10.1088/0004-637X/783/2/121](https://doi.org/10.1088/0004-637X/783/2/121)
- Gagné, J., Mamajek, E. E., Malo, L., et al. 2018, *ApJ*, 856, 23, doi: [10.3847/1538-4357/aaae09](https://doi.org/10.3847/1538-4357/aaae09)
- Gaia Collaboration, Prusti, T., de Bruijne, J. H. J., et al. 2016, *aap*, 595, A1, doi: [10.1051/0004-6361/201629272](https://doi.org/10.1051/0004-6361/201629272)
- Gaia Collaboration, Brown, A. G. A., Vallenari, A., et al. 2021, *aap*, 649, A1, doi: [10.1051/0004-6361/202039657](https://doi.org/10.1051/0004-6361/202039657)
- Gaidos, E., Mann, A. W., Rojas-Ayala, B., et al. 2022, arXiv e-prints, arXiv:2204.14163. <https://arxiv.org/abs/2204.14163>
- Gillon, M., Triaud, A. H. M. J., Demory, B.-O., et al. 2017, *at*, 542, 456, doi: [10.1038/nature21360](https://doi.org/10.1038/nature21360)
- Grankin, K. N., Bouvier, J., Herbst, W., & Melnikov, S. Y. 2008, *A&A*, 479, 827, doi: [10.1051/0004-6361:20078476](https://doi.org/10.1051/0004-6361:20078476)
- Grankin, K. N., Melnikov, S. Y., Bouvier, J., Herbst, W., & Shevchenko, V. S. 2007, *A&A*, 461, 183, doi: [10.1051/0004-6361:20065489](https://doi.org/10.1051/0004-6361:20065489)
- Guidry, J. A., Vanderbosch, Z. P., Hermes, J. J., et al. 2021, *ApJ*, 912, 125, doi: [10.3847/1538-4357/abee68](https://doi.org/10.3847/1538-4357/abee68)
- Hambálek, L., Vaňko, M., Paunzen, E., & Smalley, B. 2019, *MNRAS*, 483, 1642, doi: [10.1093/mnras/sty3151](https://doi.org/10.1093/mnras/sty3151)
- Hamilton, C. M., Herbst, W., Shih, C., & Ferro, A. J. 2001, *ApJL*, 554, L201, doi: [10.1086/321707](https://doi.org/10.1086/321707)

- Herbst, W., Herbst, D. K., Grossman, E. J., & Weinstein, D. 1994, *AJ*, 108, 1906, doi: [10.1086/117204](https://doi.org/10.1086/117204)
- Jensen, E. L. N., & Mathieu, R. D. 1997, *AJ*, 114, 301, doi: [10.1086/118475](https://doi.org/10.1086/118475)
- Jensen, E. L. N., Mathieu, R. D., & Fuller, G. A. 1996, *ApJ*, 458, 312, doi: [10.1086/176814](https://doi.org/10.1086/176814)
- Kastner, J. H., Zuckerman, B., Hily-Blant, P., & Forveille, T. 2008, *A&A*, 492, 469, doi: [10.1051/0004-6361:200810815](https://doi.org/10.1051/0004-6361:200810815)
- Kerr, R. M. P., Rizzuto, A. C., Kraus, A. L., & Offner, S. S. R. 2021, *apj*, 917, 23, doi: [10.3847/1538-4357/ac0251](https://doi.org/10.3847/1538-4357/ac0251)
- Kesseli, A. Y., West, A. A., Veyette, M., et al. 2017, *ApJS*, 230, 16, doi: [10.3847/1538-4365/aa656d](https://doi.org/10.3847/1538-4365/aa656d)
- Kimani, R., Faherty, J. K., Cruz, K. L., et al. 2021, *AJ*, 161, 277, doi: [10.3847/1538-3881/abf561](https://doi.org/10.3847/1538-3881/abf561)
- Kochanek, C. S., Shappee, B. J., Stanek, K. Z., et al. 2017, *PASP*, 129, 104502, doi: [10.1088/1538-3873/aa80d9](https://doi.org/10.1088/1538-3873/aa80d9)
- Kraus, A. L., Shkolnik, E. L., Allers, K. N., & Liu, M. C. 2014, *AJ*, 147, 146, doi: [10.1088/0004-6256/147/6/146](https://doi.org/10.1088/0004-6256/147/6/146)
- Lee, J., Song, I., & Murphy, S. 2020, *MNRAS*, 494, 62, doi: [10.1093/mnras/staa689](https://doi.org/10.1093/mnras/staa689)
- Liu, M. C., Dupuy, T. J., & Allers, K. N. 2016, *ApJ*, 833, 96, doi: [10.3847/1538-4357/833/1/96](https://doi.org/10.3847/1538-4357/833/1/96)
- Lomb, N. R. 1976, *Ap&SS*, 39, 447, doi: [10.1007/BF00648343](https://doi.org/10.1007/BF00648343)
- Luhman, K. L., & Mamajek, E. E. 2012, *ApJ*, 758, 31, doi: [10.1088/0004-637X/758/1/31](https://doi.org/10.1088/0004-637X/758/1/31)
- Lyons, J. P., Allers, K. N., Herzog, M., & Liu, M. C. 2012, in *American Astronomical Society Meeting Abstracts*, Vol. 219, American Astronomical Society Meeting Abstracts #219, 345.27
- Magnier, E. A., Schlafly, E. F., Finkbeiner, D. P., et al. 2020a, *ApJS*, 251, 6, doi: [10.3847/1538-4365/abb82a](https://doi.org/10.3847/1538-4365/abb82a)
- Magnier, E. A., Chambers, K. C., Flewelling, H. A., et al. 2020b, *ApJS*, 251, 3, doi: [10.3847/1538-4365/abb829](https://doi.org/10.3847/1538-4365/abb829)
- Magnier, E. A., Sweeney, W. E., Chambers, K. C., et al. 2020c, *ApJS*, 251, 5, doi: [10.3847/1538-4365/abb82c](https://doi.org/10.3847/1538-4365/abb82c)
- Mainzer, A., Bauer, J., Grav, T., et al. 2011, *ApJ*, 731, 53, doi: [10.1088/0004-637X/731/1/53](https://doi.org/10.1088/0004-637X/731/1/53)
- Mainzer, A., Bauer, J., Cutri, R. M., et al. 2014, *ApJ*, 792, 30, doi: [10.1088/0004-637X/792/1/30](https://doi.org/10.1088/0004-637X/792/1/30)
- Mamajek, E. E., Quillen, A. C., Pecaut, M. J., et al. 2012, *AJ*, 143, 72, doi: [10.1088/0004-6256/143/3/72](https://doi.org/10.1088/0004-6256/143/3/72)
- Marocco, F., Eisenhardt, P. R. M., Fowler, J. W., et al. 2021, *ApJS*, 253, 8, doi: [10.3847/1538-4365/abd805](https://doi.org/10.3847/1538-4365/abd805)
- McCully, C., Volgenau, N. H., Harbeck, D.-R., et al. 2018, in *Society of Photo-Optical Instrumentation Engineers (SPIE) Conference Series*, Vol. 10707, *Software and Cyberinfrastructure for Astronomy V*, ed. J. C. Guzman & J. Ibsen, 107070K
- Melis, C., Zuckerman, B., Rhee, J. H., et al. 2012, *Nature*, 487, 74, doi: [10.1038/nature11210](https://doi.org/10.1038/nature11210)
- Meng, H. Y. A., Su, K. Y. L., Rieke, G. H., et al. 2015, *ApJ*, 805, 77, doi: [10.1088/0004-637X/805/1/77](https://doi.org/10.1088/0004-637X/805/1/77)
- Moór, A., Ábrahám, P., Szabó, G., et al. 2021, *ApJ*, 910, 27, doi: [10.3847/1538-4357/abdc26](https://doi.org/10.3847/1538-4357/abdc26)
- Murphy, S. J., Mamajek, E. E., & Bell, C. P. M. 2018, *MNRAS*, 476, 3290, doi: [10.1093/mnras/sty471](https://doi.org/10.1093/mnras/sty471)
- NEOWISE Team. 2020, *NEOWISE-R Single Exposure (L1b) Source Table*, IPAC, doi: [10.26131/IRSA144](https://doi.org/10.26131/IRSA144), <https://doi.org/10.26131/irsa144>
- Newton, E. R., Irwin, J., Charbonneau, D., et al. 2016, *ApJ*, 821, 93, doi: [10.3847/0004-637X/821/2/93](https://doi.org/10.3847/0004-637X/821/2/93)
- Newton, E. R., Mondrik, N., Irwin, J., Winters, J. G., & Charbonneau, D. 2018, *AJ*, 156, 217, doi: [10.3847/1538-3881/aad73b](https://doi.org/10.3847/1538-3881/aad73b)
- Osborn, H. P., Rodriguez, J. E., Kenworthy, M. A., et al. 2017, *MNRAS*, 471, 740, doi: [10.1093/mnras/stx1249](https://doi.org/10.1093/mnras/stx1249)
- Park, W., Lee, J.-E., Contreras Peña, C., et al. 2021, *ApJ*, 920, 132, doi: [10.3847/1538-4357/ac1745](https://doi.org/10.3847/1538-4357/ac1745)
- Radigan, J., Jayawardhana, R., Lafrenière, D., et al. 2012, *ApJ*, 750, 105, doi: [10.1088/0004-637X/750/2/105](https://doi.org/10.1088/0004-637X/750/2/105)
- Radigan, J., Lafrenière, D., Jayawardhana, R., & Artigau, E. 2014, *ApJ*, 793, 75, doi: [10.1088/0004-637X/793/2/75](https://doi.org/10.1088/0004-637X/793/2/75)
- Rayner, J. T., Toomey, D. W., Onaka, P. M., et al. 2003, *PASP*, 115, 362
- Rebull, L. M., Cody, A. M., Covey, K. R., et al. 2014, *AJ*, 148, 92, doi: [10.1088/0004-6256/148/5/92](https://doi.org/10.1088/0004-6256/148/5/92)
- Reiners, A. 2009, *ApJL*, 702, L119, doi: [10.1088/0004-637X/702/2/L119](https://doi.org/10.1088/0004-637X/702/2/L119)
- Rieke, G. H., Su, K. Y. L., Melis, C., & Gáspár, A. 2021, *ApJ*, 918, 71, doi: [10.3847/1538-4357/ac0dc4](https://doi.org/10.3847/1538-4357/ac0dc4)
- Rigon, L., Scholz, A., Anderson, D., & West, R. 2017, *MNRAS*, 465, 3889, doi: [10.1093/mnras/stw2977](https://doi.org/10.1093/mnras/stw2977)
- Rodriguez, D. R., Kastner, J. H., Wilner, D., & Qi, C. 2010, *ApJ*, 720, 1684, doi: [10.1088/0004-637X/720/2/1684](https://doi.org/10.1088/0004-637X/720/2/1684)
- Rodriguez, D. R., Zuckerman, B., Kastner, J. H., et al. 2013, *ApJ*, 774, 101, doi: [10.1088/0004-637X/774/2/101](https://doi.org/10.1088/0004-637X/774/2/101)
- Rodriguez, J. E., Pepper, J., Stassun, K. G., et al. 2015, *AJ*, 150, 32, doi: [10.1088/0004-6256/150/1/32](https://doi.org/10.1088/0004-6256/150/1/32)
- Roulston, B. R., Green, P. J., & Kesseli, A. Y. 2020, *ApJS*, 249, 34, doi: [10.3847/1538-4365/aba1e7](https://doi.org/10.3847/1538-4365/aba1e7)
- Scargle, J. D. 1982, *ApJ*, 263, 835, doi: [10.1086/160554](https://doi.org/10.1086/160554)
- Schlegel, D. J., Finkbeiner, D. P., & Davis, M. 1998, *ApJ*, 500, 525
- Schmidt, S. J., Hawley, S. L., West, A. A., et al. 2015, *AJ*, 149, 158, doi: [10.1088/0004-6256/149/5/158](https://doi.org/10.1088/0004-6256/149/5/158)
- Schmidt, S. J., Shappee, B. J., van Saders, J. L., et al. 2019, *ApJ*, 876, 115, doi: [10.3847/1538-4357/ab148d](https://doi.org/10.3847/1538-4357/ab148d)

- Shappee, B. J., Prieto, J. L., Grupe, D., et al. 2014, *ApJ*, 788, 48, doi: [10.1088/0004-637X/788/1/48](https://doi.org/10.1088/0004-637X/788/1/48)
- Shkolnik, E. L., Allers, K. N., Kraus, A. L., Liu, M. C., & Flagg, L. 2017, *AJ*, 154, 69, doi: [10.3847/1538-3881/aa77fa](https://doi.org/10.3847/1538-3881/aa77fa)
- Silverberg, S. M., Kuchner, M. J., Wisniewski, J. P., et al. 2016, *ApJL*, 830, L28, doi: [10.3847/2041-8205/830/2/L28](https://doi.org/10.3847/2041-8205/830/2/L28)
- Silverberg, S. M., Wisniewski, J. P., Kuchner, M. J., et al. 2020, *ApJ*, 890, 106, doi: [10.3847/1538-4357/ab68e6](https://doi.org/10.3847/1538-4357/ab68e6)
- Simons, D. A., & Tokunaga, A. 2002, *PASP*, 114, 169, doi: [10.1086/338544](https://doi.org/10.1086/338544)
- Stauffer, J., Cody, A. M., Baglin, A., et al. 2014, *AJ*, 147, 83, doi: [10.1088/0004-6256/147/4/83](https://doi.org/10.1088/0004-6256/147/4/83)
- Tonry, J. L., Stubbs, C. W., Lykke, K. R., et al. 2012, *ApJ*, 750, 99, doi: [10.1088/0004-637X/750/2/99](https://doi.org/10.1088/0004-637X/750/2/99)
- Tonry, J. L., Denneau, L., Heinze, A. N., et al. 2018, *PASP*, 130, 064505, doi: [10.1088/1538-3873/aabadf](https://doi.org/10.1088/1538-3873/aabadf)
- Vacca, W. D., Cushing, M. C., & Rayner, J. T. 2003, *PASP*, 115, 389
- van Werkhoven, T. I. M., Kenworthy, M. A., & Mamajek, E. E. 2014, *MNRAS*, 441, 2845, doi: [10.1093/mnras/stu725](https://doi.org/10.1093/mnras/stu725)
- VanderPlas, J. T. 2018, *ApJS*, 236, 16, doi: [10.3847/1538-4365/aab766](https://doi.org/10.3847/1538-4365/aab766)
- Vos, J. M., Biller, B. A., Bonavita, M., et al. 2019, *MNRAS*, 483, 480, doi: [10.1093/mnras/sty3123](https://doi.org/10.1093/mnras/sty3123)
- Wilhelm, M. J. C., & Portegies Zwart, S. 2022, *MNRAS*, 509, 44, doi: [10.1093/mnras/stab2523](https://doi.org/10.1093/mnras/stab2523)
- Winn, J. N., Hamilton, C. M., Herbst, W. J., et al. 2006, *ApJ*, 644, 510, doi: [10.1086/503417](https://doi.org/10.1086/503417)
- Wright, E. L., et al. 2010, *AJ*, 140, 1868, doi: [10.1088/0004-6256/140/6/1868](https://doi.org/10.1088/0004-6256/140/6/1868)
- Zhang, Z., Liu, M. C., Best, W. M. J., et al. 2018, *ApJ*, 858, 41, doi: [10.3847/1538-4357/aab269](https://doi.org/10.3847/1538-4357/aab269)

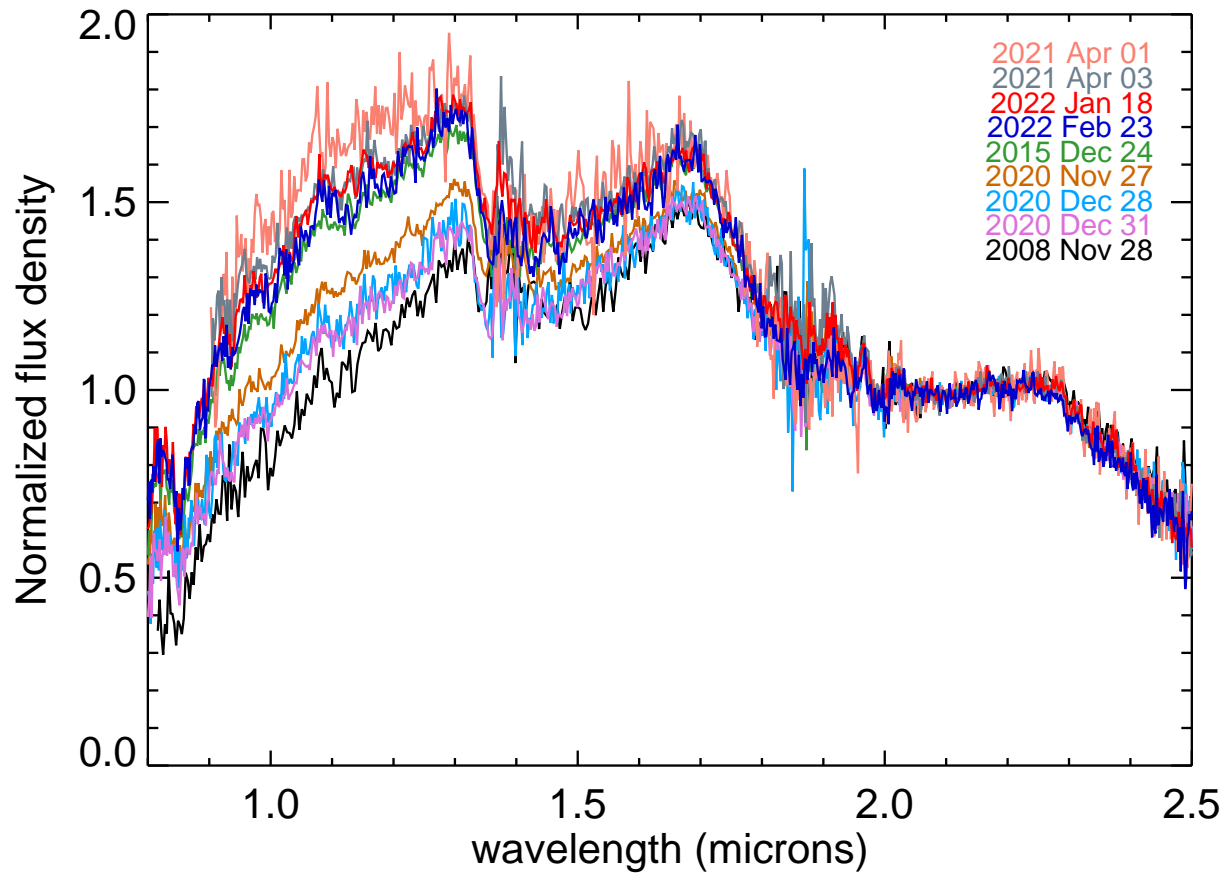


Figure 1. IRTF/Spex prism spectra of 2MASS J0619–2903, all normalized to their 2.05–2.25 μm flux. The legend with the observing dates is ordered by synthesized $J - K$ color, with the bluest epoch listed at the top.

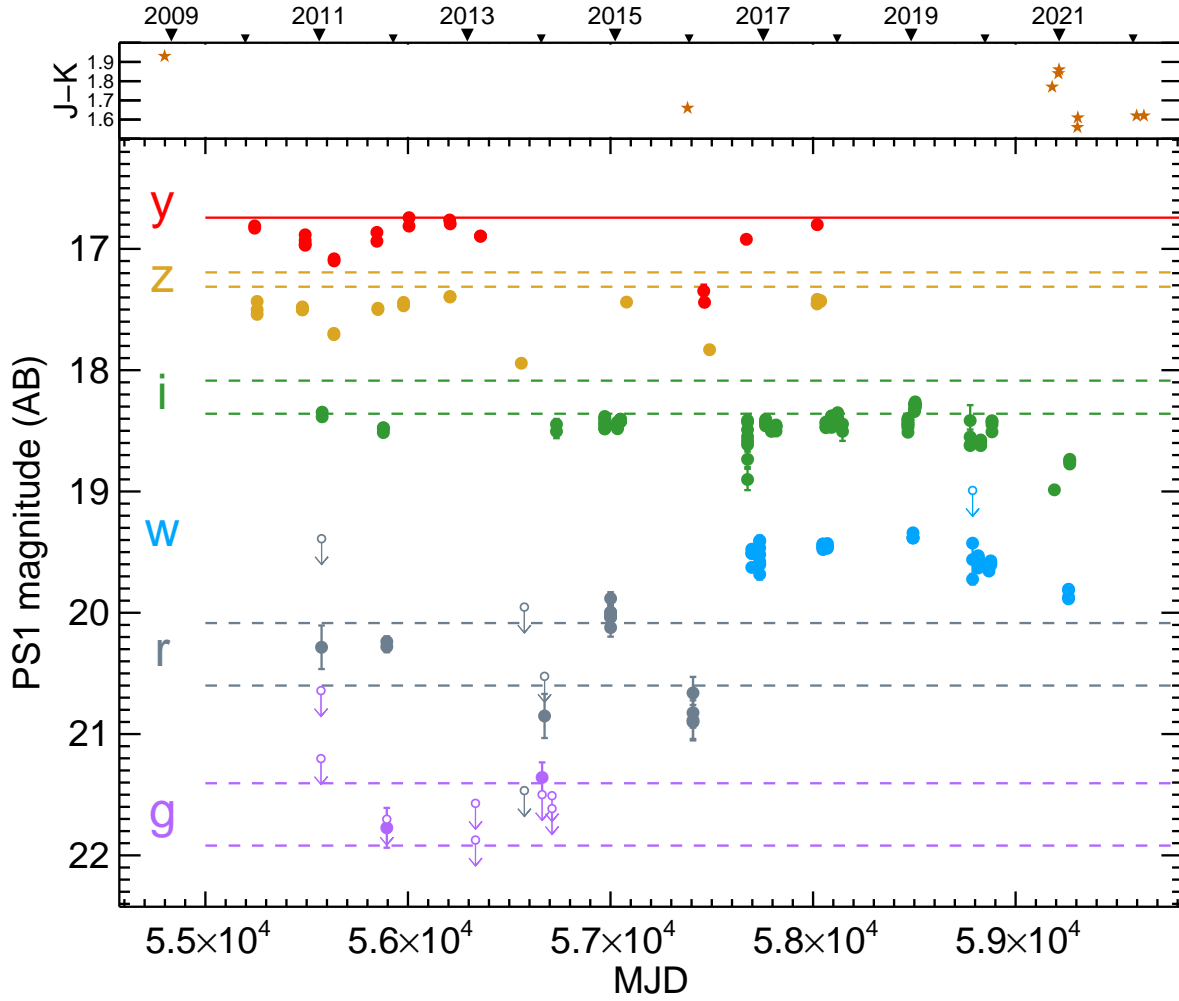


Figure 2. PS1 light curve for 2MASS J0619–2903, showing variability on timescales from sub-day to 11 years. Upper limits (5σ) are plotted as open circles with downward-pointing arrows. For reference, the dashed lines indicate the predicted 1σ range of magnitudes assuming no extinction, adopting the PS1 colors of M6 dwarfs from Best et al. (2018), and using the minimum (brightest) y_{P1} magnitude (which is shown as the solid red line) to compute magnitudes from the colors. Such color information is not available for the w_{P1} band, so there are no corresponding dashed lines for it. The small panel at the top shows the $(J - K)_{MKO}$ color synthesized from our SpeX spectra, and labels at the very top denote the start of each calendar year.

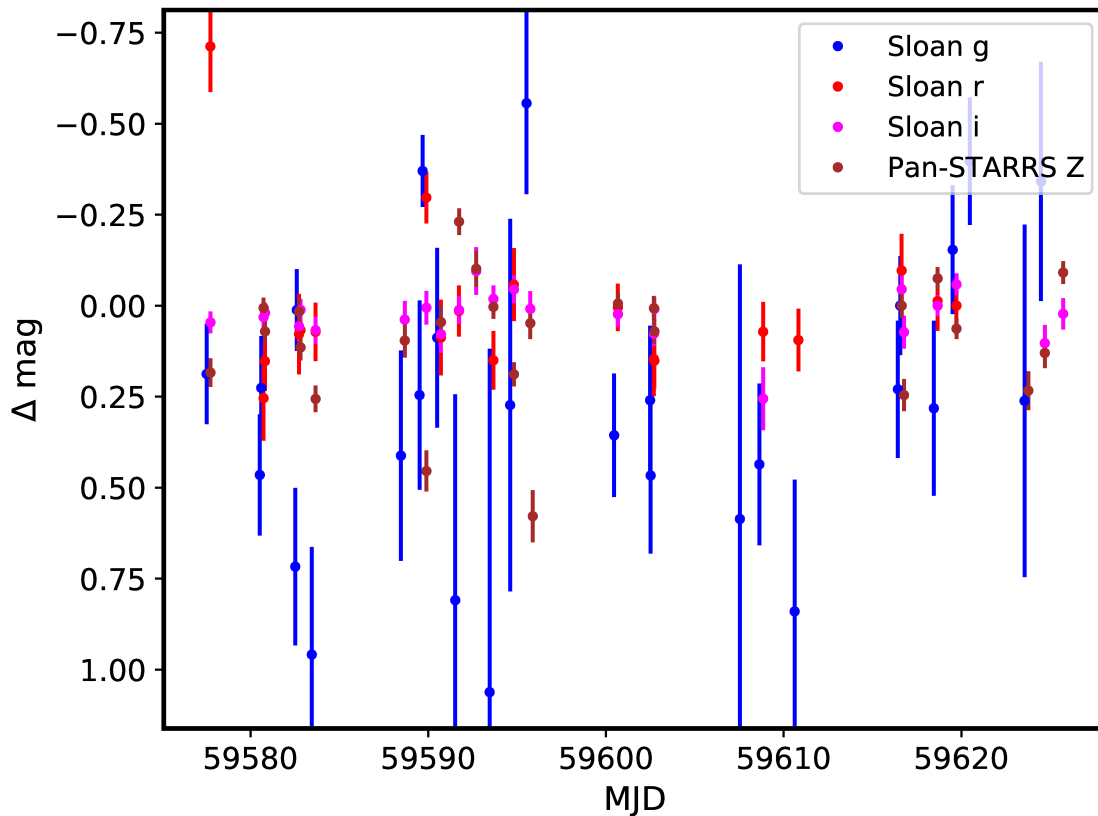


Figure 3. Optical light curves of 2MASS J0619–2903 taken with LCOGT, showing relative photometry of the source from December 2021 to February 2022. For each filter, the baseline flux is taken to be the median of the upper 50% of points and subtracted from all the epochs. The different pass-bands offset by 0.2 days for clarity. No clear evidence for variability is detected over this 1.5-month duration given the measurement uncertainties.

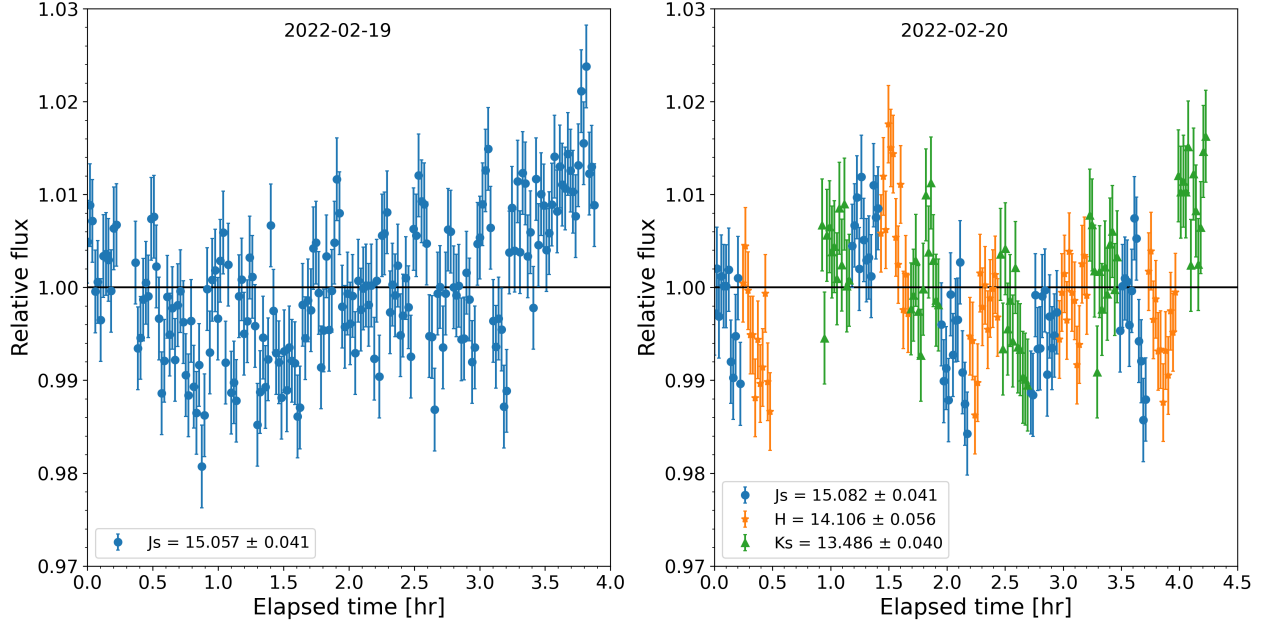


Figure 4. Near-IR light curves of 2MASS J0619–2903 taken with SOFI in J_S , H and K_S bands. The light curves show variability with an amplitude of $\approx 1\%$ over the ≈ 4 hours of observing at each night. The median magnitude of each light curve is listed in the legend, as calibrated with 2MASS stars in the field.

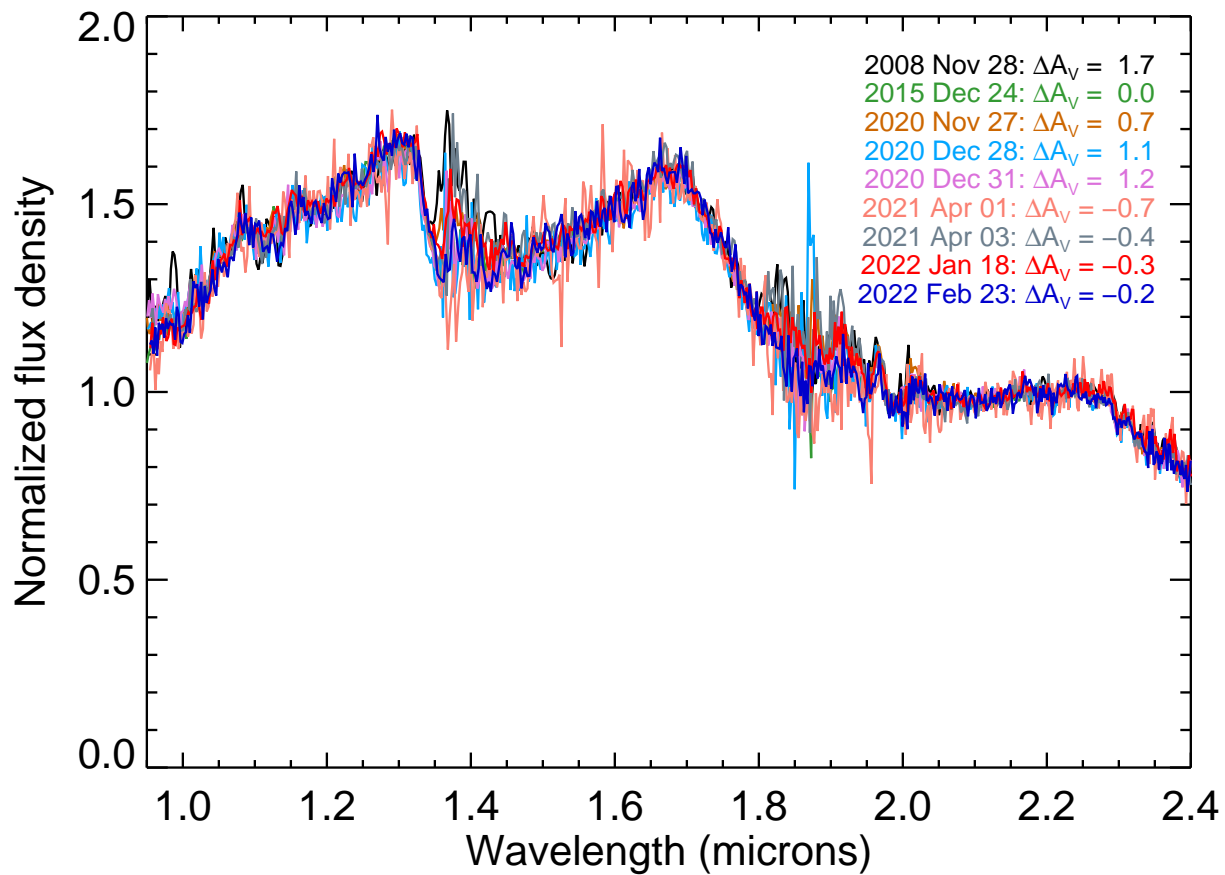


Figure 5. IRTF/SpeX prism spectra of 2MASS J0619–2903 after dereddening with the best-fitted extinction relative to the 2015 spectrum, all normalized to their 2.15–2.25 μm flux. The results are consistent with the scenario that the near-IR variability is due to changes in circumstellar extinction.

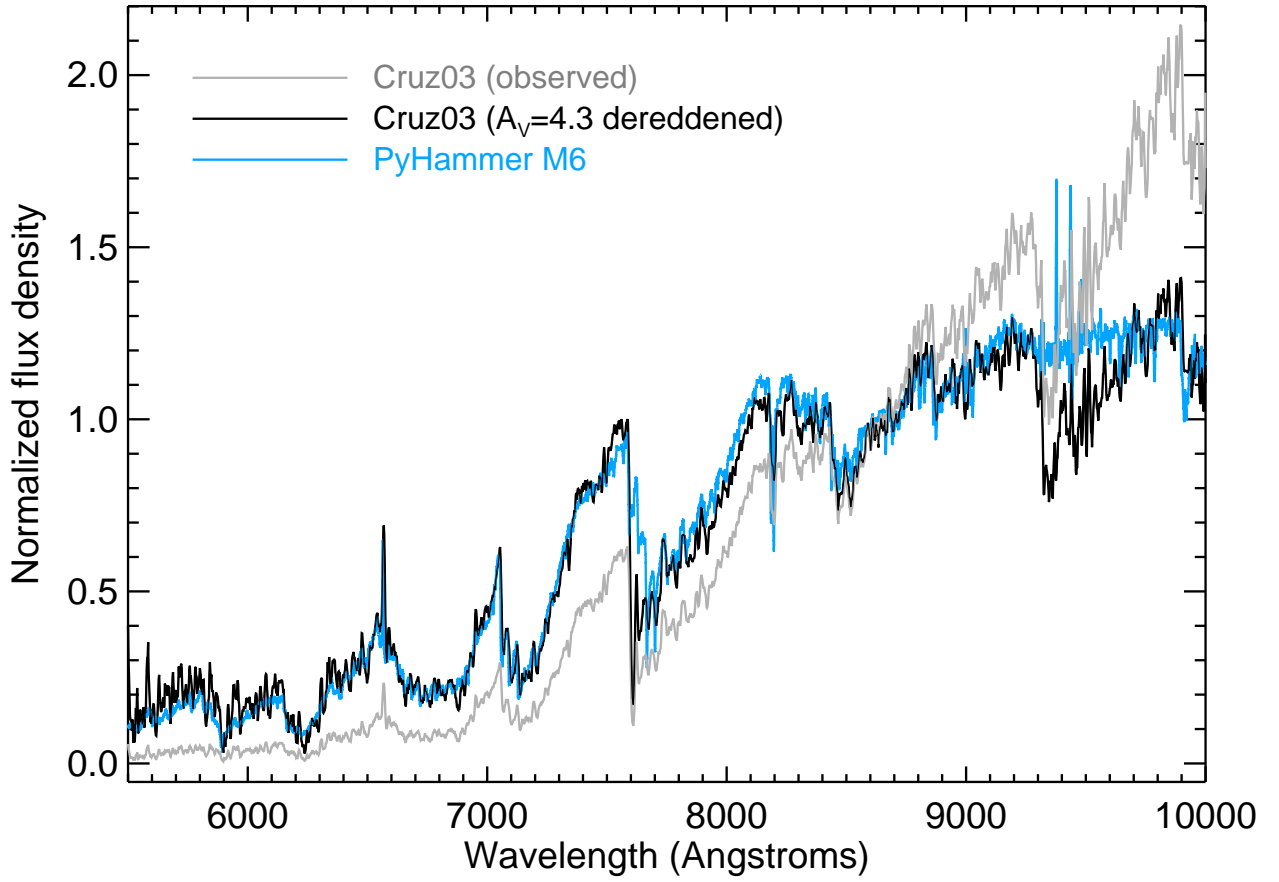


Figure 6. Comparison of 2MASS J0619–2903 optical spectrum from Cruz et al. (2003) with the solar-metallicity M6 template from PyHammer v2.0 (Roulston et al. 2020), normalized by their fluxes at 8400–8900 Å. The observed spectrum (*grey*) is significantly redder than the template. After dereddening by $A_V = 4.3$ mag, the agreement is much better. (The Cruz et al. spectra plotted here have been smoothed by a 5-pixel boxcar.)

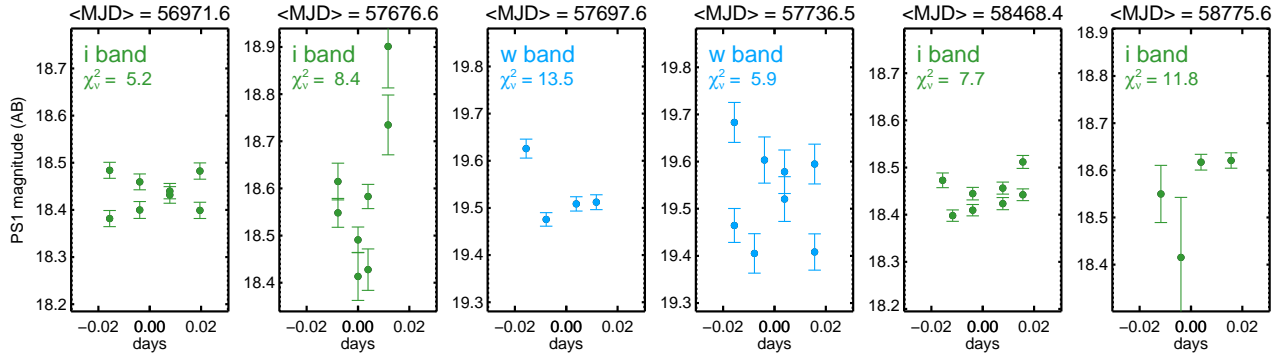


Figure 7. Possible short-timescale variability of 2MASS J0619–2903 from PS1 optical photometry, showing the 6 most variable observing blocks (defined as 4 or more detections in the same filter within a 1.5-hour window). Different colors indicate different filters, and the titles give the average Modified Julian Date for each block’s detections. The reduced χ^2 value for the photometry compared to each block’s average magnitude is also reported, all of which correspond to p -values of $< 10^{-4}$. The x - and y -axes ranges are identical in all the plots.

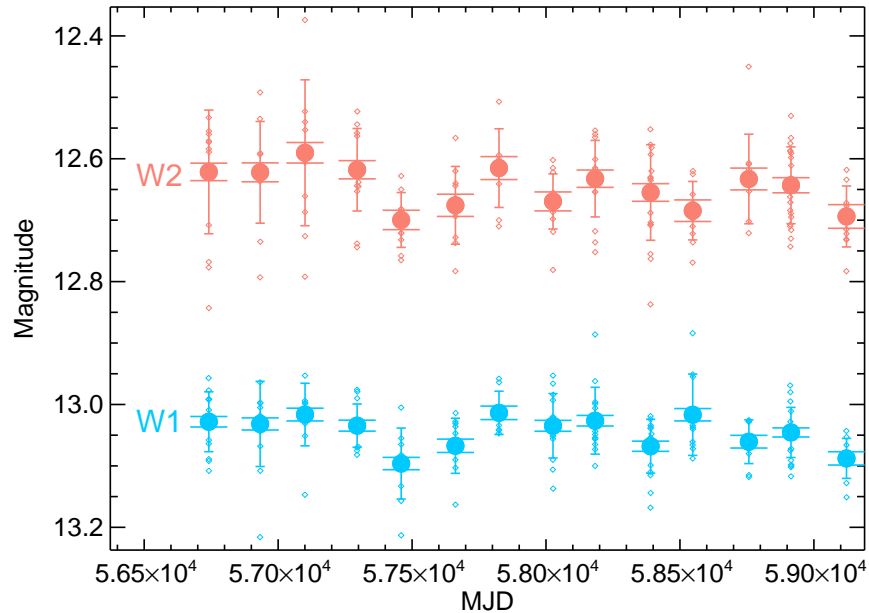


Figure 8. *NEOWISE* mid-IR light curve of 2MASS J0619–2903 from March 2014 to September 2020 using single-exposure photometry, with the weighted average at each visit plotted as a large circle with short, wide-hatted error bars. The tall, small-hatted error bars show the RMS photometric scatter at each visit. The intra-visit scatter on day-long timescales is consistent with constant flux given the measurement uncertainties, while the inter-visit scatter on 6-month timescales suggests possible ≈ 0.1 mag variability (Section 3.2.2).

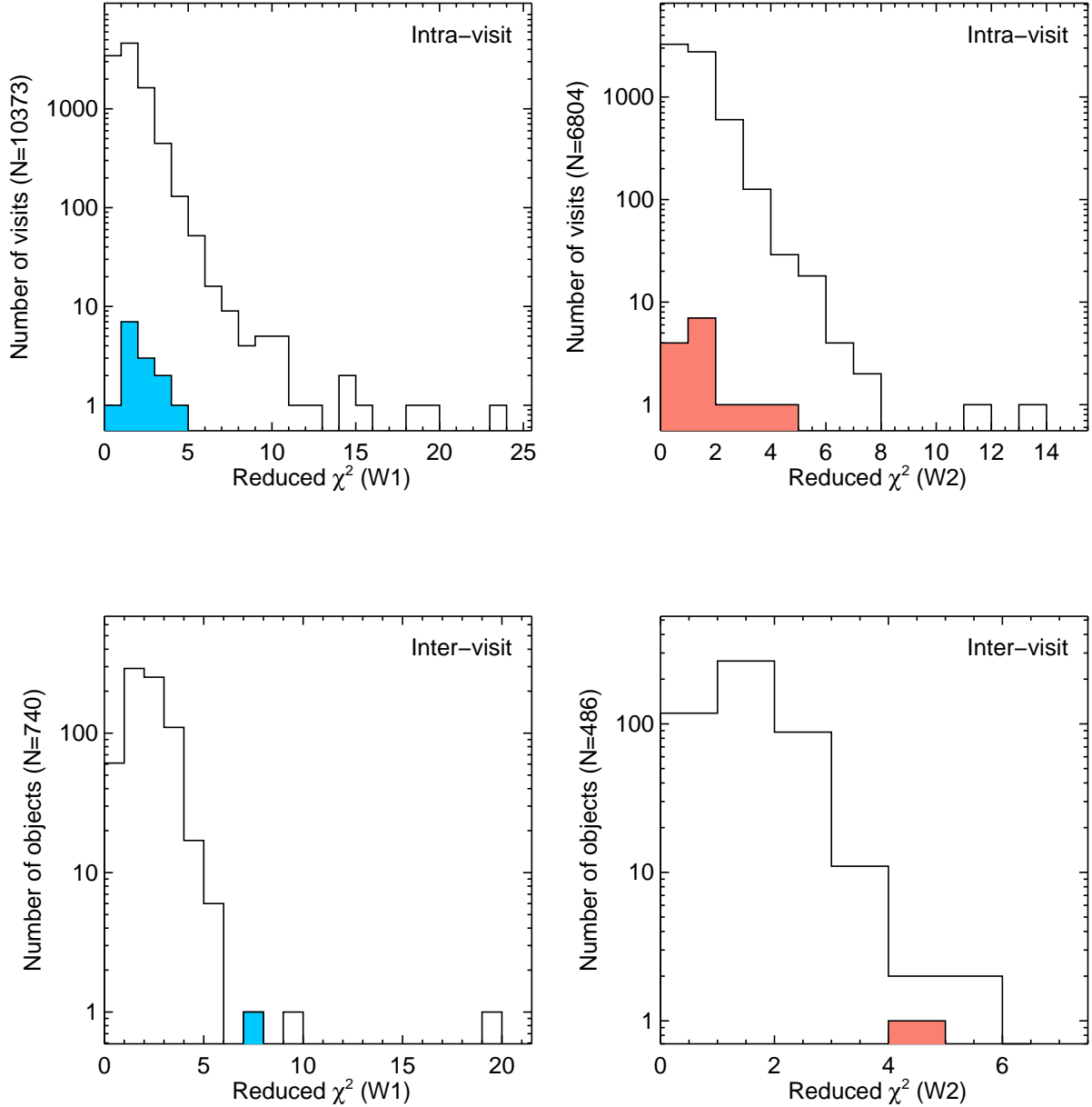


Figure 9. Comparison of 2MASS J0619–2903’s mid-IR variability compared to sources of comparable magnitude (± 0.25 mag) and within 1 deg. *Top:* Reduced χ^2 values for each day-long visit compared to a model of constant flux. (Each object has ≈ 1 dozen visits.) The histogram shows that 2MASS J0619–2903’s variations are undistinguished, i.e., no significant evidence for variability. *Bottom:* Reduced χ^2 values for each object compared to a model where the weighted averages at each visit are consistent with constant flux. 2MASS J0619–2903 has the 3rd and 4th highest $\tilde{\chi}^2$ values, suggesting possible mid-IR variability. (For all plots, note that the number of exposures and/or visits is not the same for every object, so these histograms cannot be directly compared to a specific χ^2 distribution.)

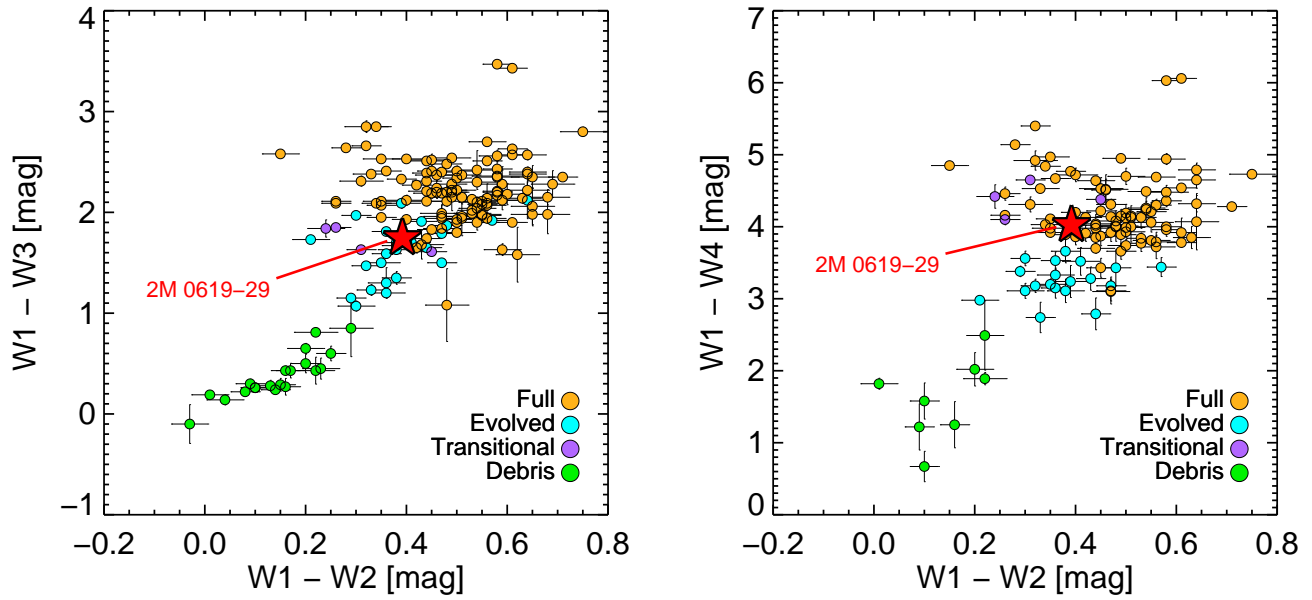


Figure 10. Comparison of the AllWISE mid-IR photometry for 2MASS J0619–2903 with disk-bearing M dwarfs in the Upper Sco region (≈ 11 Myr) from Luhman & Mamajek (2012). The colors represent different evolutionary states of the circumstellar disks. The colors show that 2MASS J0619–2903 possesses either a full or evolved disk, which is unexpected given its ≈ 30 Myr age.

Table 1. IRTF/SpEx Spectroscopy Log

Date (UT)	MJD	<Airmass>	T_{int} (s)	A0V star	Median S/N per pixel				Spectral Type	$J - K$ (mag)	Extinction	
					Y	J	H	K			ΔA_V [mag]	$\tilde{\chi}^2$
2008-11-28 ^a	54798.6	1.52	1320.0	HD 46680	21	43	41	45	M5.3±0.9 INT-G	1.93	1.74	1.2
2015-12-24 ^b	57380.4	1.71	1554.1	HD 41473	69	98	97	101	M5.8±0.9 VL-G	1.66	0.00	n/a
2020-11-27	59180.4	1.52	1554.1	HD 41473	52	71	71	65	M6.1±0.9 VL-G	1.77	0.71	1.7
2020-12-28	59211.4	1.52	777.0	HD 56751	27	39	35	40	M6.6±0.9 VL-G	1.84	1.08	1.1
2020-12-31	59214.4	2.12	1075.9	HD 50917	39	53	51	57	M5.9±0.9 VL-G	1.86	1.18	1.3
2021-04-01	59305.2	1.78	1793.2	HD 50917	20	25	18	19	M6.4±0.9 INT-G	1.56	−0.74	0.8
2021-04-03	59307.2	1.68	2630.0	HD 50917	48	60	49	54	M5.9±0.9 VL-G	1.61	−0.37	1.7
2022-01-18	59597.4	1.60	777.0	HD 43070	54	70	65	60	M5.9±0.9 VL-G	1.62	−0.32	1.6
2022-02-23	59633.3	1.73	896.6	HD 43070	35	46	39	40	M6.2±0.9 VL-G	1.62	−0.24	1.0

NOTE—For each epoch’s data, the MJD, <Airmass>, T_{int} , A0V star, and $(J - K)$ columns give the Modified Julian Date, average airmass, the total integration time, the telluric calibrator, and the synthesized $J - K$ color on the MKO photometry system (Simons & Tokunaga 2002), respectively. A conservative uncertainty estimate for the synthesized $J - K$ color would be 0.05 mag (e.g. Dupuy & Liu 2012; Radigan et al. 2012). The Extinction columns give the best-fitting relative extinction (assuming $R = 3.1$) and associated reduced χ^2 of each epoch compared to the 2015 epoch, which has the highest S/N. Negative values indicate those epochs’s spectra were bluer than the 2015 epoch. The formal errors on the fitted ΔA_V are negligible, though a conservative assumption on the overall flux calibration of the spectra would indicate an uncertainty of 0.3 mag (Section 3.1.1).

^aFrom Allers & Liu (2013).

^bFrom Liu et al. (2016).